ROTOR-BEARING SYSTEM DYNAMICS OF A HIGH SPEED MICRO END MILL SPINDLE

By

VUGAR SAMADLI

A THESIS PRESENTED TO THE GRADUATE SCHOOL
OF THE UNIVERSITY OF FLORIDA IN PARTIAL FULFILLMENT
OF THE REQUIREMENTS FOR THE DEGREE OF
MASTER OF SCIENCE

UNIVERSITY OF FLORIDA

2006

ACKNOWLEDGMENTS

I would like to first thank my advisor, Dr. N. Arakere, for guiding me through this work. I feel that I have learned much working on this project and that would not have been possible without his help. Similarly, the collaboration with Dr. J. Zeigert and Dr. L. William and their students Scott Payne, Eric Major and Andrew Riggs was fruitful. I want to thank Scott Payne for his help and it was always a friendly environment to work with him in his lab.

My company, BP Azerbaijan unit, was a main factor in making this whole effort possible so I would like to thank them all, and specifically Ralph Ladd, learning and development coordinator, and Kevin Kennelley, engineering manager.

Lastly, I would like to thank my parents because they were supportive of this effort and always encouraged my education.

TABLE OF CONTENTS

APPENDIX

LIST OF TABLES

LIST OF FIGURES

Abstract of Thesis Presented to the Graduate School
of the University of Florida in Partial Fulfillment of the
Requirements for the Degree of Master of Science

ROTOR-BEARING SYSTEM DYNAMICS OF A HIGH
SPEED MICRO END MILL SPINDLE

By

Vugar Samadli

August 2006

Chair: Nagaraj Arakere
Major Department: Mechanical and Aerospace Engineering

Current micro-scale manufacturing technologies find limited application in a wide range of high strength engineering materials because of the difficulties encountered in creating complex three dimensional structures and features. Although milling is one of the most widely used processes for this type of manufacturing at the macro scale, it has yet to become an economically viable technology for micro-scale manufacturing. For optimal chip formation using very small diameter cutters, and to achieve economical material removal rates combined with good surface finish, high spindle speeds are needed. In addition, a low runout is desired to prevent premature tool breakage. However, the lack of suitable spindles capable of achieving rotational speeds in excess of 500,000 rpm coupled with sub-micrometer runout at the tool tip makes micro-scale milling commercially unviable.

This thesis demonstrates several means of analyzing the rotor dynamic behavior of a spindle in order to find critical speeds, unbalance response and linear stability margins. Experimental testing is performed to estimate bearing dynamic behavior at high speed.

The results of this study provide parameters for bearing stiffness and damping, bearing span and balancing limits to achieve sub-micrometer runout of tool tip for speeds upto 1 million rpm.

CHAPTER 1
INTRODUCTION

The technology development in the field of miniaturization has become a global phenomenon. Its impact is far and widespread across a broad application domain that encompasses many diverse fields and industries, such as telecommunications, portable consumer electronics, defense, and biomedical. The perfect example is the field of computers where modern computers which possess greater processing power and can fit under a desk or on a lap have replaced the bulky computers of the past such as the ENIAC (electronic numerical integrator and computer) which once filled large rooms. In recent times, more and more attention is being paid to the issues involved in the design, development, operation, and analysis of the equipment and processes of manufacturing micro components since the global trend toward the increased integration of miniaturized technology into society has gained enormous momentum. Currently, common techniques utilized in the fabrication of micro-components are based on the techniques developed for the silicon wafer processing industry. Unfortunately these processes are limited to production of simple planar geometries in a narrow range of material and are cost effective only in large volume [1]. Even though non traditional fabrication methods, such as focused ion beam machining, laser machining, and electrodischarge machining, are capable of producing high-precision micro-components, they have limited potential as mass production techniques due to the high initial cost, poor productivity, and limited material selection [2]. Micro milling has the potential to fabricate micro components and is capable of machining complex 3D shapes from wide variety of shapes and materials.

The objective of this research is to develop a micro-milling spindle which will rotate at over 500,000 rpm range with sub-micrometer runout, and thus become a commercially usable and cost effective manufacturing technology. Most machine tools such as lathes, milling machines, and all types of grinding machines, use a spindle or an axis of rotation for positioning work pieces or tools or machining parts and thus a large part of their accuracy can be attributed to the spindle. Consequently, the accuracy of the spindles used in their design directly influences the accuracy of the entire machine and thus can be considered as one of the most important components in the overall accuracy and operation of a machine tool.

Most commercial micro-tools have a 1/8th inch diameter shank (see Figure 1-1). This must be of utmost importance when designing the micro spindle. Another functional requirement is the ease of tool changing with minimal time and effort. The only viable way to meet the above design requirements while still obtaining satisfactory runout is to concentrate on designs incorporating the use of tool shank itself as the spindle shaft. To achieve desired performance, the following three functions must be satisfied:

1. Bearing subsystem. The bearing system must be so designed that it meets the following requirements. Firstly and fore mostly, it must be capable of supporting the tool shank without causing excessive runout. Also, it must support both radial and axial loads, and support rapid tool changes. Flexure Pivot Tilting Pad Bearings (FPTPB) are being studied as a potential bearing subsystem.

2. Drive subsystem. The tool drive system must be able to drive the tool at the required speed with enough torque and power to perform the desired machining operations. Also it should not introduce disturbance forces that cause excessive tool point runout. These requirements make air turbine drive as a potential drive subsystem. The system would incorporate the turbine blades directly into the tool shank of the micro-tool.

3. Monitoring subsystem. Theoretical and scientific understanding of micro-milling requires monitoring and recording of cutting forces. However, in the measurement bandwidth (that is 1,000,000 rpm with a 2-flute cutter and tooth passing frequency

of 33 KHz), the force measurement is extremely difficult because of the high frequencies encountered even though the cutting forces are low.

The goals of this project are the following:

- To extend the capability to model and predict rotordynamics and bearing behavior at small sizes and high speeds.

- Development of a procedure for identification of dynamic stiffness and damping coefficients for the bearing.

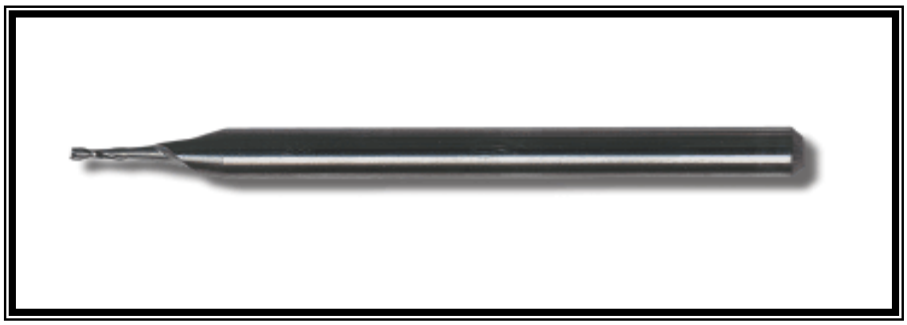

Figure 1-1. Commercial micro-tool

CHAPTER 2
DEVELOPMENT OF EQUATION OF MOTION OF ROTOR-BEARING SYSTEM AND PARAMETER IDENTIFICATION

It is of utmost importance in many companies that not only the operation should be uninterrupted and reliable but also it should be carried out at high power and high speed. Another vital requirement is the accurate prediction and control of the dynamic behavior (unbalance response, critical speeds and instability). These factors were the motivations for this research wherein rigid rotor analysis and finite element analysis was used to investigate bearing coefficient parameters and the rotordynamics of micro spindle. Both the rigid rotor analysis and finite element analysis have been performed simultaneously. The tungsten carbide spindle has a first bending or flexure natural frequency of 2.2 million rpm for a bearing span of 1 inch. The spindle operating speeds are expected to be about 500,000 rpm. Hence rigid rotor analysis can be justified. Finally, the experimental setup was designed to find bearing parameters which were compared with analytical results.

2.1 Rigid Rotor Analysis

In order to get generalized rotor dynamic models, the Jeffcott rotor is extended to a four degree of freedom rigid rotor system as shown in the schematic diagram of Figure 2-1. The four coordinates, which are the two geometric center translations (V, W) and the two rotation angles (B, Γ) describe the rotor configuration relative to the fixed reference (X, Y, Z). Bearing 1 and bearing 2 are located at an axial distance a_1 and a_2 from the

center of mass, respectively. Both these distances are defined as positive in the plus X direction. The rotor configuration is always defined so that a_1 is positive.

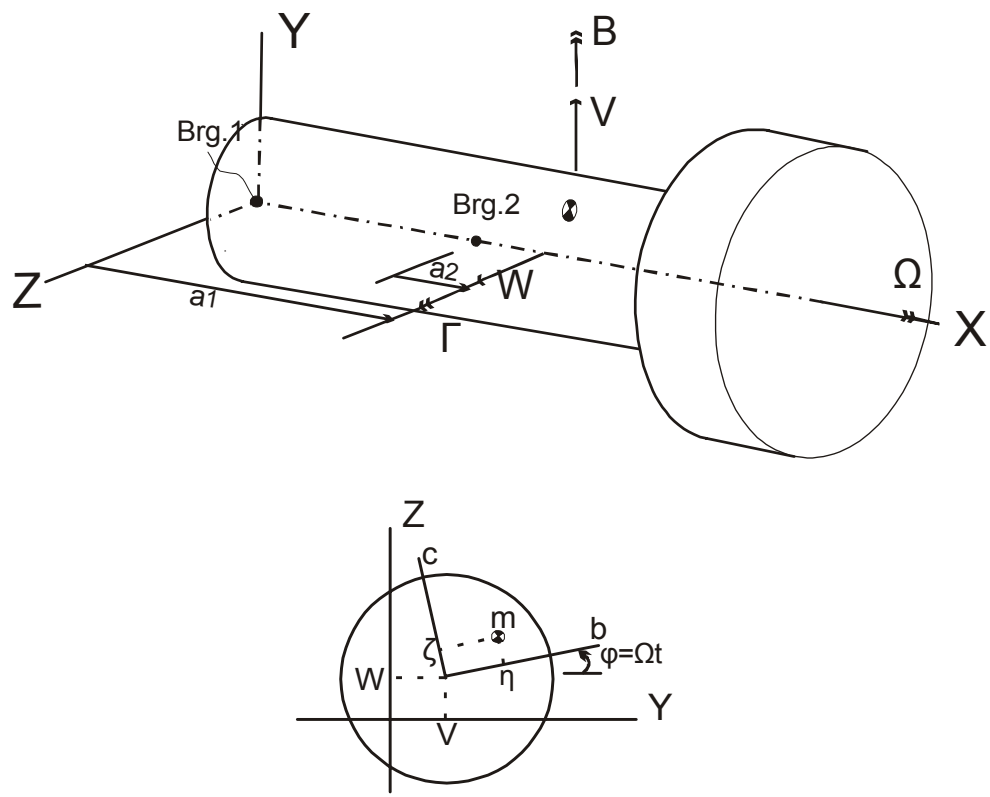

Figure 2-1. Rigid rotor schematic.

Where

(a, b, c)	geometric center body reference
(η, ζ)	eccentricity components
(φ)	spin angle = Ωt
(Ω)	constant spin frequency

$$
\begin{aligned}
V_m(t) &= V + (\eta\cos\varphi - \zeta\sin\varphi) \\
W_m(t) &= W + (\zeta\cos\varphi + \eta\sin\varphi)
\end{aligned}
\tag{2-1}
$$

The angular rate of the rigid body is

$$
\begin{aligned}
\omega_a &= \Omega - \dot{\Gamma}\sin \mathrm{B} \\
\omega_b &= \dot{\Gamma}\cos \mathrm{B}\sin\Omega t + \dot{\mathrm{B}}\cos\Omega t \\
\omega_c &= \dot{\Gamma}\cos \mathrm{B}\cos\Omega t - \dot{\mathrm{B}}\sin\Omega t
\end{aligned}
\tag{2-2}
$$

and the kinetic energy of the rigid body is

$$T = \frac{1}{2} m(\dot{V}_m{}^2 + \dot{W}_m{}^2) + \frac{1}{2}\left[I_p \omega_a{}^2 + I_d(\omega_b{}^2 + \omega_c{}^2) \right] \tag{2-3}$$

By considering the variational work of the bearing forces, they are included in the equation of motion. The bearing force is a function of lateral shaft translations and velocities at the bearing location.

$$\begin{aligned} F_Y &= F_Y(V, W, \dot{V}, \dot{W}) \\ F_Z &= F_Z(V, W, \dot{V}, \dot{W}) \end{aligned} \tag{2-4}$$

Upon Taylor's series expansion of eq. (2-4) about the origin, the force components in eq. (2-4) are approximated by their corresponding linear forms. At the ith typical bearing, forces are expressed in the following equation:

$$\begin{bmatrix} F_Y \\ F_Z \end{bmatrix} = -\begin{bmatrix} k_{iYY} & k_{iYZ} \\ k_{iZY} & k_{iZZ} \end{bmatrix} \begin{bmatrix} V_i \\ W_i \end{bmatrix} - \begin{bmatrix} c_{iYY} & c_{iYZ} \\ c_{iZY} & c_{iZZ} \end{bmatrix} \begin{bmatrix} \dot{V}_i \\ \dot{W}_i \end{bmatrix} \tag{2-5a}$$

or

$$\bar{F}_i = -\underline{k}_i \bar{r}_i - \underline{c}_i \dot{\bar{r}}_i \tag{2-5b}$$

where

$$\bar{r}_i = \begin{bmatrix} 1 & 0 & 0 & -a_i \\ 0 & 1 & a_i & 0 \end{bmatrix} \bar{q} = \underline{A}_i \bar{q} \tag{2-6}$$

$$\bar{q}^T = \begin{bmatrix} V & W & B & \Gamma \end{bmatrix} \tag{2-7}$$

.

The variational work done by bearing forces on the rotor is given by the following expression

$$\delta W_k = \sum_{i=1}^{2} \bar{F}_i \delta \bar{r}_i = \sum_{k=1}^{4} Q_k \delta q_k \tag{2-8}$$

where Q_k represents the generalized bearing forces.

Lagrange's equations are of the following form:

$$\frac{d}{dt}\left(\frac{\partial T}{\partial \dot{q}_k}\right) - \frac{\partial T}{\partial q_k} = Q_k \qquad k=1,2,3,4 \tag{2-9}$$

Using the above set of equations and inserting in eq (2-9) the following set of rigid rotor equations of motion has been obtained:

$$\underline{M}\ddot{\overline{q}} + (\underline{C} - \Omega\underline{G})\dot{\overline{q}} + \underline{K}\overline{q} = \overline{Q} \tag{2-10}$$

where

$$\underline{M} = \begin{bmatrix} m & 0 & 0 & 0 \\ 0 & m & 0 & 0 \\ 0 & 0 & I_d & 0 \\ 0 & 0 & 0 & I_d \end{bmatrix} \qquad \underline{G} = \begin{bmatrix} 0 & 0 & 0 & 0 \\ 0 & 0 & 0 & 0 \\ 0 & 0 & 0 & -I_p \\ 0 & 0 & I_p & 0 \end{bmatrix}$$

$$\underline{K} = \sum_{i=1}^{2} \underline{A}_i^T \underline{k}_i \underline{A}_i \qquad \underline{C} = \sum_{i=1}^{2} \underline{A}_i^T \underline{c}_i \underline{A}_i$$

$$\overline{Q} = m\Omega^2 \begin{bmatrix} \eta \\ \zeta \\ 0 \\ 0 \end{bmatrix} \cos\Omega t + m\Omega^2 \begin{bmatrix} -\zeta \\ \eta \\ 0 \\ 0 \end{bmatrix} \sin\Omega t \tag{2-11}$$

2.2 Finite Element Analysis

Typically, it is not possible to obtain analytical solutions for problems involving complicated geometries, loadings and material properties. Based on the study and inspection of various approaches available for modeling, one of the most appropriate methods for modeling of high-speed micro spindle is the FEA, finite element method. It is also the only feasible type of computer simulation available for this purpose. The finite element method is generally a numerical method used for solving engineering and mathematical physics problems. The following steps are used in the FEA for dynamic response solution [3]:

- Form element stiffness matrix.
- Form element mass matrix.
- Assemble system stiffness matrix and incorporate constraints.
- Assemble system mass matrix and incorporate constraints.
- Solve eigenproblem and obtain a vector of frequencies and mode shapes.
- Form excitation vector in physical coordinates.

2.3 Identifying Bearing Parameters By Experimental Method

The estimation of the dynamic bearing characteristics using theoretical methods usually results in an error in the prediction of the dynamic behavior of rotor-bearing systems. Reliable estimates of the bearing operating condition in actual test conditions are difficult to obtain and, therefore to reduce the discrepancy between the measurements and the prediction, physically meaningful and accurate parameter identification is required in actual test conditions. There are some similarities between various experimental methods for the dynamic characterization of rolling element bearings, fluid-film bearings and magnetic bearings. These methods require forces as input signals and displacement/velocities/accelerations of the dynamic system to be measured are usually the output signals, and input-output relationships are used to determine the unknown parameters of the system models. There are a lot of identification techniques of bearing parameters, which are based on methods used to excite the system [4], such as the following:

1. Methods using Incremental Static Load
2. Methods using Dynamic Load
3. Methods using an Excited Load
4. Method using Unbalance Mass

5. Methods using an Impact Hammer
6. Methods using Unknown Excitation

Appendix A summarizes the source material on the experimental dynamic parameter identification of bearings.

2.3.1 Methods Using Incremental Static Load

Mitchell et al. (1965-66) [5] performed experiments to incrementally load the bearing and measuring the change in position, and obtained the four stiffness coefficients of fluid-film bearings. They obtained the following simple relationships using the influence coefficient approach to

$$k_{yy} = \alpha_{zz} / \gamma \qquad k_{yz} = -\alpha_{yz} / \gamma$$
$$k_{zy} = -\alpha_{zy} / \gamma \qquad k_{zz} = \alpha_{yy} / \gamma \tag{2-12}$$

where

$$\gamma = \alpha_{yy}\alpha_{zz} - \alpha_{yz}\alpha_{zy}$$

$$\alpha_{yy} = y_1 / \Delta F_y \qquad \alpha_{zy} = z_1 / \Delta F_y$$
$$\alpha_{yz} = y_2 / \Delta F_z \qquad \alpha_{zz} = z_2 / \Delta F_z \tag{2-13}$$

Here y_1 and z_1 are displacements of the journal center from its static equilibrium position in vertical and horizontal directions respectively, on the application of a static incremental load ΔF_y in the vertical direction; and y_2 and z_2 are displacements corresponding to a static incremental load ΔF_z in the horizontal direction. This method can be applied to any type of bearing since the estimation of stiffness requires the establishment of a relationship between the force and the corresponding displacement.

2.3.2 Methods Using Dynamic Load

Dynamic load methods have been the most researched and widely used in the identification of dynamic bearing parameters in the last 45 years [4]. Their major

advantages are that they can be readily implemented on a real machine and the excitation can be applied either to the journal or to the bearing housing depending on practical constraints.

For the rigid rotor case, when the excitation is applied to the journal (Figure 2-2), the fluid-film dynamic equation can be written as

$$\begin{bmatrix} m_{yy} & m_{yz} \\ m_{zy} & m_{zz} \end{bmatrix} \begin{Bmatrix} \ddot{y} \\ \ddot{z} \end{Bmatrix} + \begin{bmatrix} c_{yy} & c_{yz} \\ c_{zy} & c_{zz} \end{bmatrix} \begin{Bmatrix} \dot{y} \\ \dot{z} \end{Bmatrix} + \begin{bmatrix} k_{yy} & k_{yz} \\ k_{zy} & k_{zz} \end{bmatrix} \begin{Bmatrix} y \\ z \end{Bmatrix} = \begin{Bmatrix} f_y - m(\ddot{y} + \ddot{y}_B) \\ f_z - m(\ddot{z} + \ddot{z}_B) \end{Bmatrix} \tag{2-14}$$

where m is the mass of the journal, y and z represent the motion of the journal center from its equilibrium position relative to the bearing center, and y_B and z_B are the components of the absolute displacement of the bearing center in vertical and horizontal directions, respectively. In this case, the origin of the coordinate system is assumed to be at the static equilibrium position, so that gravity does not appear explicitly in the equation of motion. There will be one equation of this form for each of the bearings and the terms y_B, z_B represent the motion of the supporting structure. For the case of a rigid rotor with bearings on a rigid support, equation (2-14) can be expressed in the form

$$M_B\ddot{q} + C_B\dot{q} + K_B q = f - M_R\ddot{q} \tag{2-15}$$

The subscripts R and B refer to the rotor and bearings, respectively. On collecting the terms together, we get

$$(M_B + M_R)\ddot{q} + C_B\dot{q} + K_B q = f \tag{2-16}$$

The overall system mass, damping and stiffness matrices can be formed by adding the separate contributions of the bearings and rotor in equation (2-16). This form was used by Arumugam et al. (1995) [6] to extract K_B and C_B in terms of the known and measurable quantities such as the rotor model, forcing and corresponding response. The

sinusoidal response of a rotor at speed Ω is studied using the modified form of this equation (2-16), and the response is of the form

$$q = Qe^{j\Omega t}$$

The governing equation of motion is given by

$$\left[-M\Omega^2 + j\Omega C + K\right]Q = F_u = \left[Z(\Omega)\right]Q \tag{2-17}$$

where [Z(Ω)] is the dynamic stiffness matrix, F_u is the unbalance force, and Ω is the rotational frequency of the rotor.

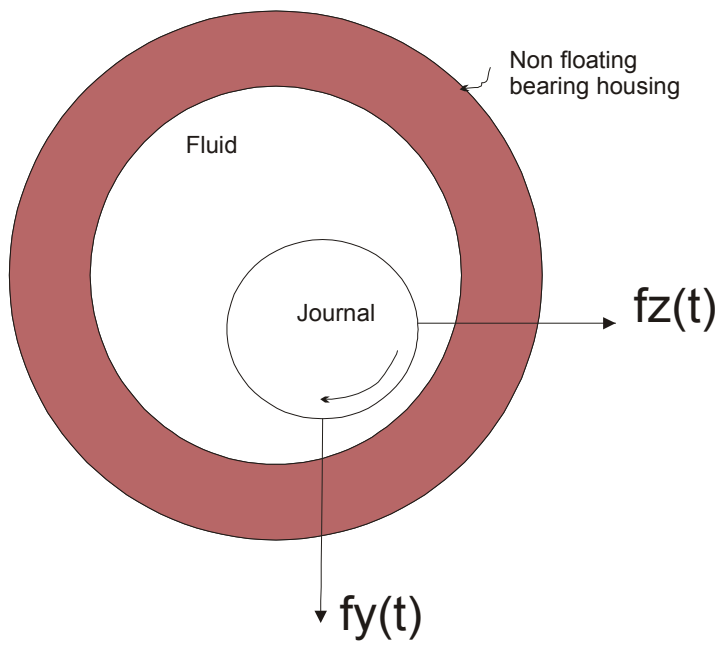

Figure 2-2. A non-floating bearing housing and a rotating journal.

2.3.3 Methods Using an Excitation Force

The application of a calibrated force to the journal can only rarely be applied in practical situations. Glienicke (1966–67) [7] adopted the technique of exciting the floating bearing bush (housing) sinusoidally in two mutually perpendicular directions (Figure 2-3) and measuring the amplitude and phase of the resulting motions in each case. The stiffness and damping coefficients were then calculated from the frequency-domain equations.

Morton (1971) [8] devised a measurement using the receptance coefficient method procedure for the estimation of the dynamic bearing characteristics. He excited the lightweight floating bearing bush by using very low forcing frequencies, ω (10 and 15 Hz). Assuming the inertia force due the fluid film and bearing housing masses to be negligible, and for sinusoidal motion, equation (2-14) may be written as

$$\begin{bmatrix} z_{yy} & z_{yz} \\ z_{zy} & z_{zz} \end{bmatrix} \begin{Bmatrix} Y \\ Z \end{Bmatrix} = \begin{Bmatrix} F_y \\ F_z \end{Bmatrix}$$

with (2-18)

$$z = k + j\omega c$$

where Y and Z are complex displacements and F_y and F_z are complex forces in the vertical and horizontal directions, respectively. In equation (2-18) k represents the effective bearing stiffness coefficient, since while estimating the bearing dynamic stiffness, z, the fluid-film added-mass and journal mass effects contribute to the real part of the dynamic stiffness and the effective stiffness is estimated.

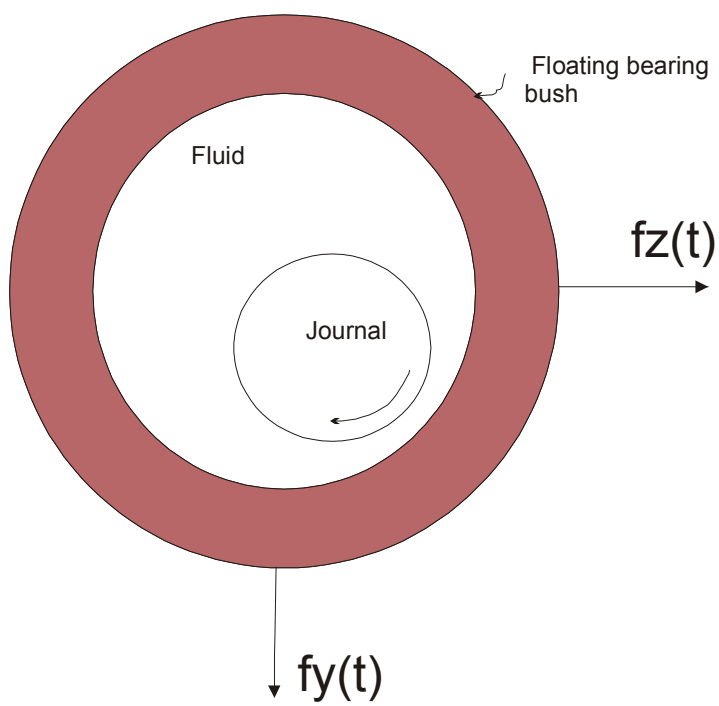

Figure 2-3. A floating bearing housing and a fixed rotating shaft.

Someya (1976) [9], Hisa et al. (1980) [10] and Sakakida et al. (1992) [11] identified the dynamic coefficients of large-scale journal bearings by using simultaneous sinusoidal excitations on the bearing at two different frequencies and measuring the corresponding displacement responses. This is called the two-directional compound sinusoidal excitation method and all eight bearing dynamic coefficients can be obtained from a single test. When the journal is vibrating about the equilibrium position in a bearing, the dynamic component of the reaction force of the fluid film can be expressed by equation (2-18). If the excitation force and dynamic displacement are measured at two different excitation frequencies under the same static state of equilibrium and ignoring the fluid-film added-mass effects equation (2-18) can be solved for the eight unknown coefficients as

$$\begin{bmatrix} Y_1 & Z_1 & j\omega_1 Y_1 & j\omega_1 Z_1 \\ Y_2 & Z_2 & j\omega_2 Y_2 & j\omega_2 Z_2 \end{bmatrix} \begin{Bmatrix} k_{yy} \\ k_{yz} \\ c_{yy} \\ c_{yz} \end{Bmatrix} = \begin{Bmatrix} F_{y1} - m_B \omega_1^2 Y_{B1} \\ F_{y2} - m_B \omega_2^2 Y_{B2} \end{Bmatrix}$$

$$\begin{bmatrix} Y_1 & Z_1 & j\omega_1 Y_1 & j\omega_1 Z_1 \\ Y_2 & Z_2 & j\omega_2 Y_2 & j\omega_2 Z_2 \end{bmatrix} \begin{Bmatrix} k_{zy} \\ k_{zz} \\ c_{zy} \\ c_{zz} \end{Bmatrix} = \begin{Bmatrix} F_{z1} - m_B \omega_1^2 Z_{B1} \\ F_{z2} - m_B \omega_2^2 Z_{B2} \end{Bmatrix} \tag{2-19}$$

where ω is the external excitation frequency and the subscripts 1 and 2 represent the measurements corresponding to two different excitation frequencies. Since equation (2-19) corresponds to eight real equations, the bearing dynamic coefficients can be obtained on substituting the measured values of the complex quantities Fy, Fz, Y, Z, Y_B and Z_B,

2.3.4 Method Using Unbalance Mass

From a practical point of view, the simplest method of excitation is to use an unbalance force as this requires no sophisticated equipment for the excitation, and it is relatively easy to identify the rotational speed dependency of the bearing dynamic characteristics. However, the disadvantage is that information is limited to the synchronous response. Nevertheless, since this is the predominant requirement, the application of forces due to unbalance is extremely useful. Hagg and Sankey (1956, 1958) [12-13] were among the first to use the unbalance force only for experimentally measuring the oil-film elasticity and damping for the case of a full journal bearing. They used the experimental measurement technique of Stone and Underwood (1947) [14] in which they used the vibration diagram to measure the vibration amplitude and phase of the journal motion relative to the bearing housing. The direct stiffness and damping coefficients were only considered along the principal directions in their study (i.e., major and minor axes of the journal elliptical orbit).

The measured unbalance response whirl orbit gives the stiffness and damping coefficients. However, the results represent some form of effective rotor-bearing coefficients and not the true film coefficients as the cross-coupled coefficients are ignored. Duffin and Johnson (1966–67) [15] employed a similar approach to that of Hagg and Sankey to identify bearing dynamic coefficients of large journal bearings. They proposed an iterative procedure to calculate all eight coefficients. Four equations can be written relating the measured values of displacement amplitude and phase Y, Z, φ_y and φ_z, together with the known value of the unbalance force, F, and four stiffness coefficients (obtained from static locus curve method; Mitchell et al., 1965–66) used to obtain the four unknown damping coefficients. This allows the solution of two sets of

simultaneous equations having two equations in each set. The results had a greater accuracy than the method (Glienecke, 1966–67) in which two sets of four simultaneous equations were used to obtain the stiffness and damping coefficients.

Murphy and Wagner (1991) [16] presented a method using a synchronously orbiting intentionally eccentric journal as the sole source of excitation for the extraction of stiffness and damping coefficients for hydrostatic bearings. The relative whirl orbits across the fluid film were made to be elliptic with asymmetric stiffness in the test bearing's supporting structure. The study considered the bearing coefficients to be skew-symmetric and the elliptic nature was utilized in the data reduction process. Adams et al. (1992) [17] and Sawicki et al. (1997) [18] utilized experimentally measured responses corresponding to at least three discrete orbital frequencies, for a given operating condition to obtain twelve dynamic coefficients (stiffness, damping and added-mass) of hydrostatic and hybrid journal bearings, respectively. They assumed that the bearing dynamic coefficients are independent of frequency of excitation. The estimation equation was similar to equation (2-19) except the rotor mass was ignored and fluid film added-mass coefficients were considered. A confidence in the measurements was obtained by employing dual piezoelectric/strain gage load/displacement measuring systems. The difference between these two sets of dynamic force measurements was typically less than 2%. The test spindle (double-spool-shaft) had a provision for a circular orbit motion of adjustable magnitude with independent control over spin speed, orbit frequency and whirl direction. The least-squares linear regression fit to all frequency data points over the tested frequency range was used to obtain the bearing dynamic coefficients.

2.3.5 Methods Using an Impact Hammer

Until the early 1970s, the common method to obtain the dynamic characteristics of systems involved using sinusoidal excitation [4]. Downham and Woods (1971) [19] proposed a technique using a pendulum hammer to apply an impulsive force to a machine structure. Although they were interested in vibration monitoring rather than the determination of bearing coefficients, their work led to the idea that impulse testing could be capable of exciting all the modes of a linear system.

Nordmann (1975) [20] and Nordmann and Schöllhorn (1980) [21] identified the stiffness and damping coefficients of journal bearings by modal testing by means of the impact method wherein, a rigid rotor, running in journal bearings was excited by an impact hammer. Two independent impacts first in the vertical direction and then in the horizontal direction were applied to the rotor and the corresponding responses were measured. A transformation of input signals (forces) and output signals (displacements of the rotor) into the frequency domain was then carried out and the four complex FRFs were calculated. The bearing dynamic parameters were assumed to be independent of the frequency of excitation. The analytical FRFs, which depend on the bearing dynamic coefficients, were fitted to the measured FRFs. An iterative fitting process results in the stiffness and damping coefficients.

Zhang et al. (1992a) [22] fitted the measured FRFs to those calculated theoretically so as to obtain the eight bearing dynamic coefficients. They also quantitatively analyzed the influence of noise and measurement errors on the estimation in order to improve the accuracy of estimated bearing dynamic coefficients. They used a half-sinusoid impulse excitation and with a different level of noise added to the resulting response to test their algorithm and averaged the frequency responses to reduce the uncertainty due to noise in

the response. To reduce the effect of phase-measurement errors, they defined an error function using just the amplitude components of the FRFs. This non-linear objective function was then used to estimate the bearing parameters by an iterative procedure. It was also demonstrated by then that it was necessary to remove the unbalance response from the signal when an impact test was used, especially at higher speeds of operation, and they concluded this to be the reason for the scatter in the results by impact excitation, as compared to the discrete frequency harmonic excitation.

This method is time-consuming though since impact tests have to be conducted for each rotor speed at which bearing dynamic parameters are desired. In general, the amount of information that can be extracted from a single impulse test is limited as the governing equations for a bearing include coupling between the two perpendicular directions. Errors in the estimation will be greater for the case when bearing dynamic coefficients are functions of external excitation frequency as compared to the estimation from functions of rotor rotational frequency. Also impulse testing may lead to underestimation of input forces when applied to a rotating shaft as a result of the generation of friction-related tangential force components and, further, is prone to poor signal-to-noise ratios because of the high crest factor.

2.3.6 Methods Using Unknown Excitation

In industrial machinery, the application of a calibrated force is difficult to apply. Due to residual unbalance, misalignment, rubbing between the rotor and stator, aerodynamic forces, oil whirl, oil whip and instability, inherent forces are present in the system and these render the assessment of the forcing impossible. Adams and Rashidi (1985) [23] used the static loading method to measure bearing stiffness coefficients and determined orbital motion at an adjustable threshold speed to extract bearing damping

coefficients by inverting the associated eigenproblem. The approach stems from the physical requirement for an exact internal energy balance between positive and negative damping influences at an instability threshold. The approach was illustrated by simulation and does not require the measurement of dynamic forces.

Lee and Shih (1996) [24] found rotor parameters including bearing dynamic coefficients, shaft unbalance distribution and disk eccentricity in flexible rotors by presenting an estimation procedure based on the transfer matrix method. The relations between measured response data and the known system parameters were used to formulate the normal equations. The parameter estimation was then performed using the least squares method by assuming that the bearing dynamic coefficients were constant at close spin speeds.

CHAPTER 3
ROTOR DYNAMIC ANALYSIS OF MICRO SPINDLE

The aim of this project is to rotate a spindle supported by air bearings at up to 500,000 rpm, with sub-micrometer runout. The 1/8th inch diameter tool shank is used as a spindle shaft. As mentioned before, the only viable way to obtain satisfactory runout was to use the tool shank itself as the spindle shaft. An air turbine is used as a driving system for the spindle. Thus, the only viable way to assemble air turbine is to manufacture the turbine integral with the spindle, which is shown in Figure 3-1. Also from the practicality point of view the micro-spindle must accept a variety of tools with minimal time and effort required for tool change. Rotordynamics of high-speed flexible shafts is influenced by the complex interaction between the unbalance forces, bearing stiffness and damping, inertial properties of the rotor, gyroscopic stiffening effects, aerodynamic coupling, and speed-dependent system critical speeds. For stable high-speed operations, bearings must be designed with the appropriate stiffness and damping properties, selected on the basis of a detailed rotordynamic analysis of the rotor system. The two types of rotor dynamic analyses that are used for high-speed thin spindle are rigid rotor analysis and finite element analysis. The dynamic behavior of a spindle is analyzed in order to find critical speeds, unbalance response and linear stability margins by these methods.

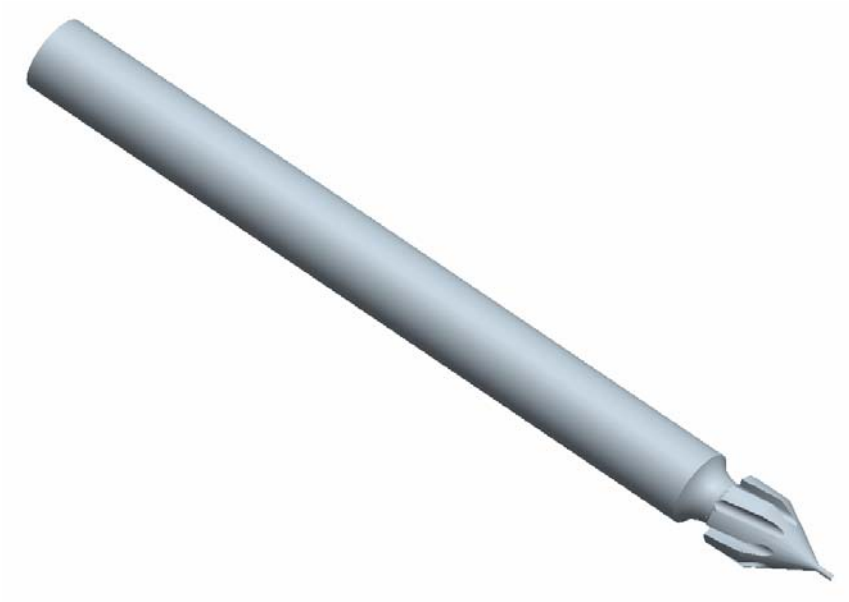

Figure 3-1. Micro-spindle.

3.1 Rigid Rotor Analysis

Rigid rotor analysis was initially used to get the rotor unbalance response. The air bearings were located on either side of the center of mass, as shown in Figure 3-2. In addition, center of mass is found by solid model ProE software.

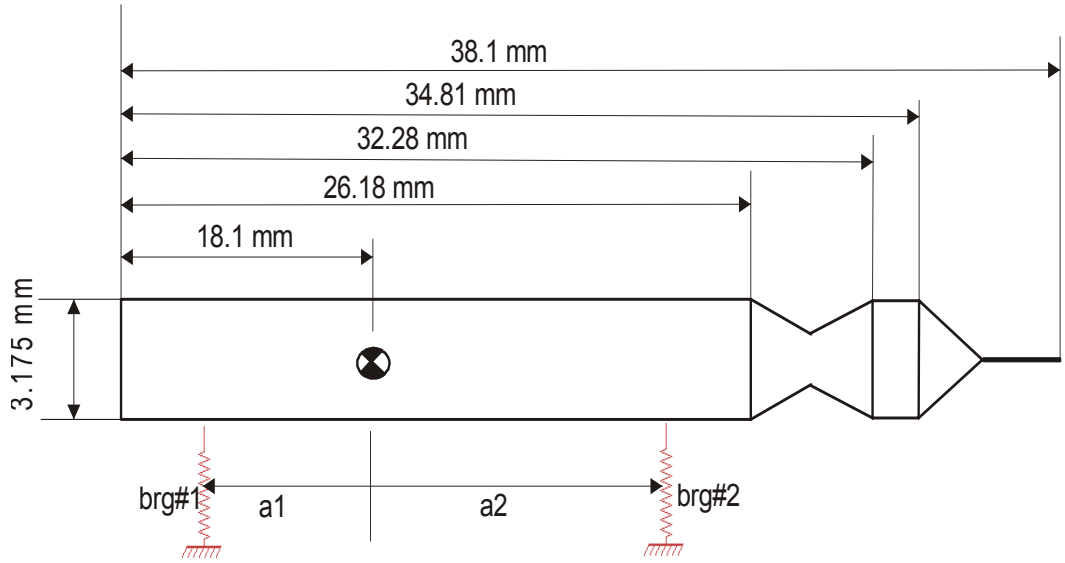

Figure 3-2. Bearings location on spindle.

The rigid rotor has 4 degrees of freedom (DOF) represented by two displacements (V, W) and two rotations (B, Γ) of the center of mass. The following equation, (derivation can be found in chapter 2), was used for a rigid rotor subjected to unbalance.

$$\underline{M}\ddot{\bar{q}} + (\underline{C} - \Omega\underline{G})\dot{\bar{q}} + \underline{K}\bar{q} = \bar{Q} \tag{2-1}$$

where $\underline{M}$, $\underline{C}$, $\underline{G}$, $\underline{K}$ are mass, damping, gyroscopic and stiffness matrices, respectively, $\bar{Q}$ is the force vector. Expressions of these matrices can be found in chapter 2. Ω is constant spin frequency.

In order to use equation (2-1) in the rotor orbit analysis, following procedure is applied. From chapter 2, it is known that displacement vector for 4 DOF is the following:

$$\bar{q}^T = \begin{bmatrix} V & W & B & \Gamma \end{bmatrix}$$

The shaft unbalance leads to harmonic synchronous excitation. Hence the displacement or response vector can be expressed as the following:

$$\bar{q} = \begin{Bmatrix} V_C \\ W_C \\ B_C \\ \Gamma_C \end{Bmatrix} \cos(\Omega t) + \begin{Bmatrix} V_S \\ W_S \\ B_S \\ \Gamma_S \end{Bmatrix} \sin(\Omega t) \tag{3-1}$$

As a result, first and second derivatives will have the following forms, respectively.

$$\dot{\bar{q}} = -\Omega \begin{Bmatrix} V_C \\ W_C \\ B_C \\ \Gamma_C \end{Bmatrix} \sin(\Omega t) + \Omega \begin{Bmatrix} V_S \\ W_S \\ B_S \\ \Gamma_S \end{Bmatrix} \cos(\Omega t) \tag{3-2}$$

$$\ddot{\bar{q}} = -\Omega^2 \begin{Bmatrix} V_C \\ W_C \\ B_C \\ \Gamma_C \end{Bmatrix} \cos(\Omega t) - \Omega^2 \begin{Bmatrix} V_S \\ W_S \\ B_S \\ \Gamma_S \end{Bmatrix} \sin(\Omega t) \tag{3-3}$$

After substituting for $\underline{M}$, $\underline{C}$, $\underline{G}$, $\underline{K}$, Q into equation (2-1) using (3-1), (3-2), (3-3) and rearranging sine and cosine terms, and using harmonic balance, the following expression can been obtained:

$$
\begin{bmatrix}
k^1_{yy}+k^2_{yy}-m\Omega^2 & k^1_{yz}+k^2_{yz} & a_1k^1_{yz}+a_2k^2_{yz} & -(a_1k^1_{yy}+a_2k^2_{yy}) & \Omega(c^1_{yy}+c^2_{yy}) & \Omega(c^1_{yz}+c^2_{yz}) & \Omega(a_1c^1_{yz}+a_2c^2_{yz}) & \Omega(a_1c^1_{yy}+a_2c^2_{yy}) \\
k^1_{zy}+k^2_{zy} & k^1_{zz}+k^2_{zz}-m\Omega^2 & a_1k^1_{zz}+a_2k^2_{zz} & -(a_1k^1_{zy}+a_2k^2_{zy}) & \Omega(c^1_{zy}+c^2_{zy}) & \Omega(c^1_{zz}+c^2_{zz}) & \Omega(a_1c^1_{zz}+a_2c^2_{zz}) & \Omega(a_1c^1_{zy}+a_2c^2_{zy}) \\
a_1k^1_{zy}+a_2k^2_{zy} & a_1k^1_{zz}+a_2k^2_{zz} & a_1^2k^1_{yy}+a_2^2k^2_{zz}-\Omega^2\mathrm{I}_d & -(a_1^2k^1_{zy}+a_2^2k^2_{zy}) & \Omega(a_1c^1_{zy}+a_2c^2_{zy}) & \Omega(a_1c^1_{zz}+a_2c^2_{zz}) & \Omega(a_1^2c^1_{yy}+a_2^2c^2_{zz}) & -\Omega(a_1^2c^1_{zy}+a_2^2c^2_{zy}) \\
-(a_1k^1_{yy}+a_2k^2_{yy}) & -(a_1k^1_{yz}+a_2k^2_{yz}) & -(a_1^2k^1_{yz}+a_2^2k^2_{yz}) & a_1^2k^1_{zz}+a_2^2k^2_{zz}-\Omega^2\mathrm{I}_d & -\Omega(a_1c^1_{yy}+a_2c^2_{yy}) & -\Omega(a_1c^1_{yz}+a_2c^2_{yz}) & -\Omega(a_1^2c^1_{yz}+a_2^2c^2_{yz}) & \Omega(a_1^2c^1_{zz}+a_2^2c^2_{zz}) \\
-\Omega(c^1_{yy}+c^2_{yy}) & -\Omega(c^1_{yz}+c^2_{yz}) & \Omega(a_1c^1_{yz}+a_2c^2_{yz}) & \Omega(a_1c^1_{yy}+a_2c^2_{yy}) & k^1_{yy}+k^2_{yy}-m\Omega^2 & k^1_{yz}+k^2_{yz} & a_1k^1_{yz}+a_2k^2_{yz} & -(a_1k^1_{yy}+a_2k^2_{yy}) \\
-\Omega(c^1_{zy}+c^2_{zy}) & -\Omega(c^1_{zz}+c^2_{zz}) & \Omega(a_1c^1_{zz}+a_2c^2_{zz}) & \Omega(a_1c^1_{zy}+a_2c^2_{zy}) & k^1_{zy}+k^2_{zy} & k^1_{zz}+k^2_{zz}-m\Omega^2 & a_1k^1_{zz}+a_2k^2_{zz} & -(a_1k^1_{zy}+a_2k^2_{zy}) \\
-\Omega(a_1c^1_{zy}+a_2c^2_{zy}) & -\Omega(a_1c^1_{zz}+a_2c^2_{zz}) & \Omega(a_1c^1_{yy}+a_2c^2_{zz}) & \Omega(a_1^2c^1_{zy}+a_2^2c^2_{zy})+\Omega^2\mathrm{I}_p & a_1k^1_{zy}+a_2k^2_{yy} & a_1k^1_{zz}+a_2k^2_{zz} & a_1^2k^1_{yy}+a_2^2k^2_{zz}-\Omega^2\mathrm{I}_d & -(a_1^2k^1_{zy}+a_2^2k^2_{zy}) \\
\Omega(a_1c^1_{yy}+a_2c^2_{yy}) & \Omega(a_1c^1_{yz}+a_2c^2_{yz}) & \Omega(a_1^2c^1_{yz}+a_2^2c^2_{yz})-\Omega^2\mathrm{I}_p & -\Omega(a_1c^1_{zz}+a_2c^2_{zz}) & -(a_1k^1_{yy}+a_2k^2_{yy}) & -(a_1k^1_{yz}+a_2k^2_{yz}) & -(a_1^2k^1_{yz}+a_2^2k^2_{yz}) & a_1^2k^1_{zz}+a_2^2k^2_{zz}-\Omega^2\mathrm{I}_d
\end{bmatrix}
$$

$$
\begin{Bmatrix} V_C \\ W_C \\ B_C \\ \Gamma_C \\ V_S \\ W_S \\ B_S \\ \Gamma_S \end{Bmatrix} = m\Omega^2 \begin{Bmatrix} \eta \\ \zeta \\ 0 \\ 0 \\ -\zeta \\ \eta \\ 0 \\ 0 \end{Bmatrix} \tag{3-4}
$$

where a1 and a2 are the distance of the bearings from center of mass. k_{yy}, k_{yz}, k_{zy}, k_{zz}, and c_{yy}, c_{yz}, c_{zy} and c_{zz} are stiffness and damping coefficients of each bearing, respectively. I_d and I_p are the polar and diametric inertia, respectively.

The charts from 'Rotor-Bearing Dynamics Design Technology' [25], design handbook for fluid film type bearings were initially used to evaluate the damping and the stiffness coefficients. In order to use these charts, bearing length and diameter ratio was assumed to be two. Mass and gyroscopic matrices were found by hand calculation, which were later entered in the MathCAD program. The two types of forces on the system are the unbalance force and the cutting force. As the cutting force is much smaller than the unbalance force, it was neglected. An unbalance eccentricity of e_u=0.000002 inch was used initially to evaluate the unbalance force. The solution procedure was implemented in MathCAD to find the unbalance respond at the bearing locations.

The rotor orbits at the two bearing supports at 500,000 rpm for a rotor with a mass=2.525×10^{-5} lbf-sec^2/in, Ip=4.187×10^{-6} lbf-sec^2-in, Id=4.894×10^{-8} lbf-sec^2-in and an unbalance eccentricity of 0.000002 inch are shown in Figure 3-3. The air bearing for this configuration has the following parameters, Table3-1.

Table 3-1. Bearing parameters at 500,000 rpm (Ω=52360 rad/sec).

$K_{yy1,2}$=950.4 lbf/in	$C_{yy1,2}$=0.021 lbf-sec/in
$K_{yz1,2}$=99.1 lbf/in	$C_{yz1,2}$=-0.004 lbf-sec/in
$K_{zy1,2}$=93.46 lbf/in	$C_{zy1,2}$=0.005 lbf-sec/in
$K_{zz1,2}$=1050.4 lbf/in	$C_{zz1,2}$=0.106 lbf-sec/in

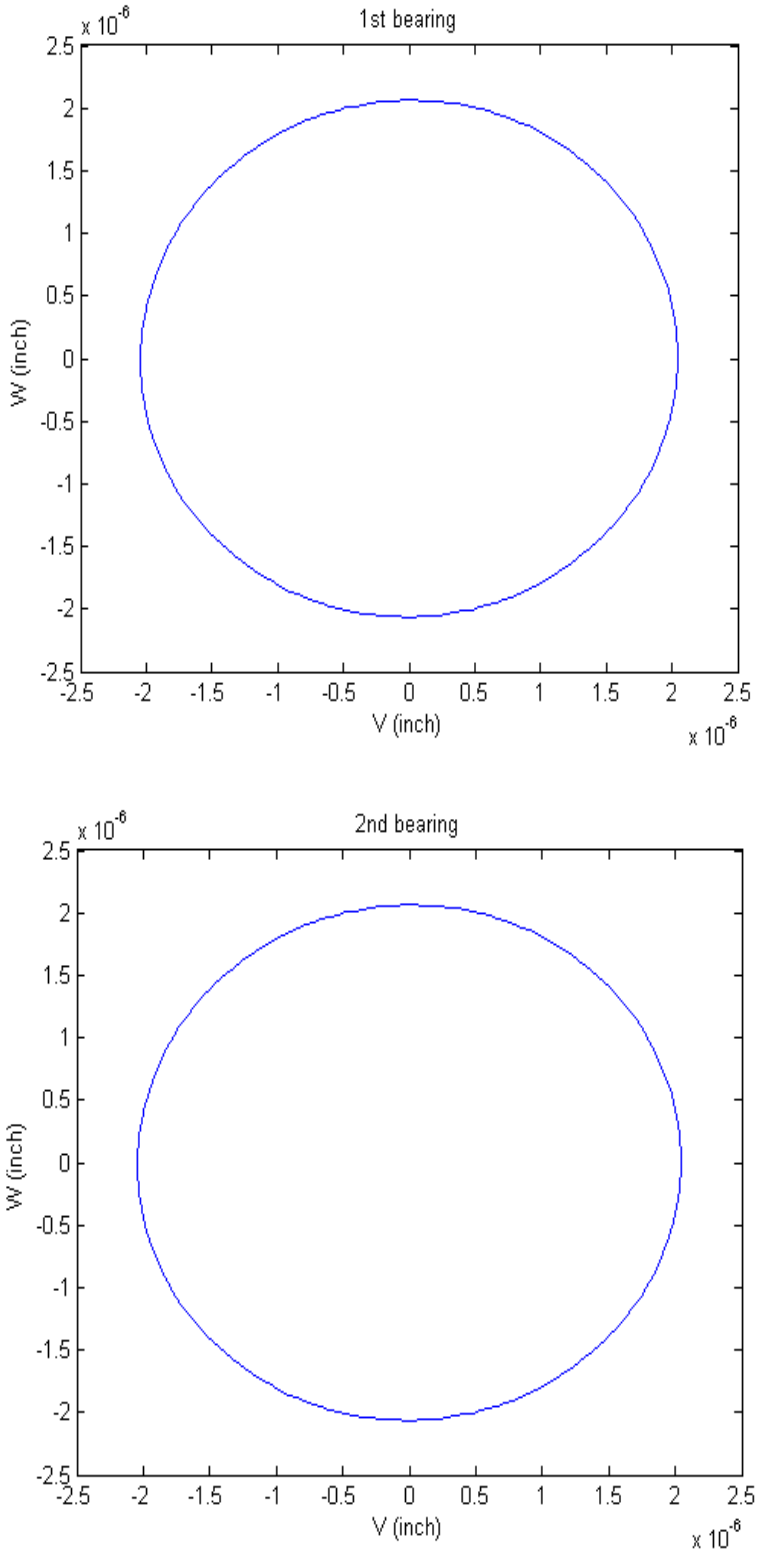

Figure 3-3. Rotor orbits at two bearing supports at 500,000 rpm.

Even for the 1,000,000 rpm and same tool with same rigid rotor parameters, displacement of rotor in bearings is small (see figure 3-4).

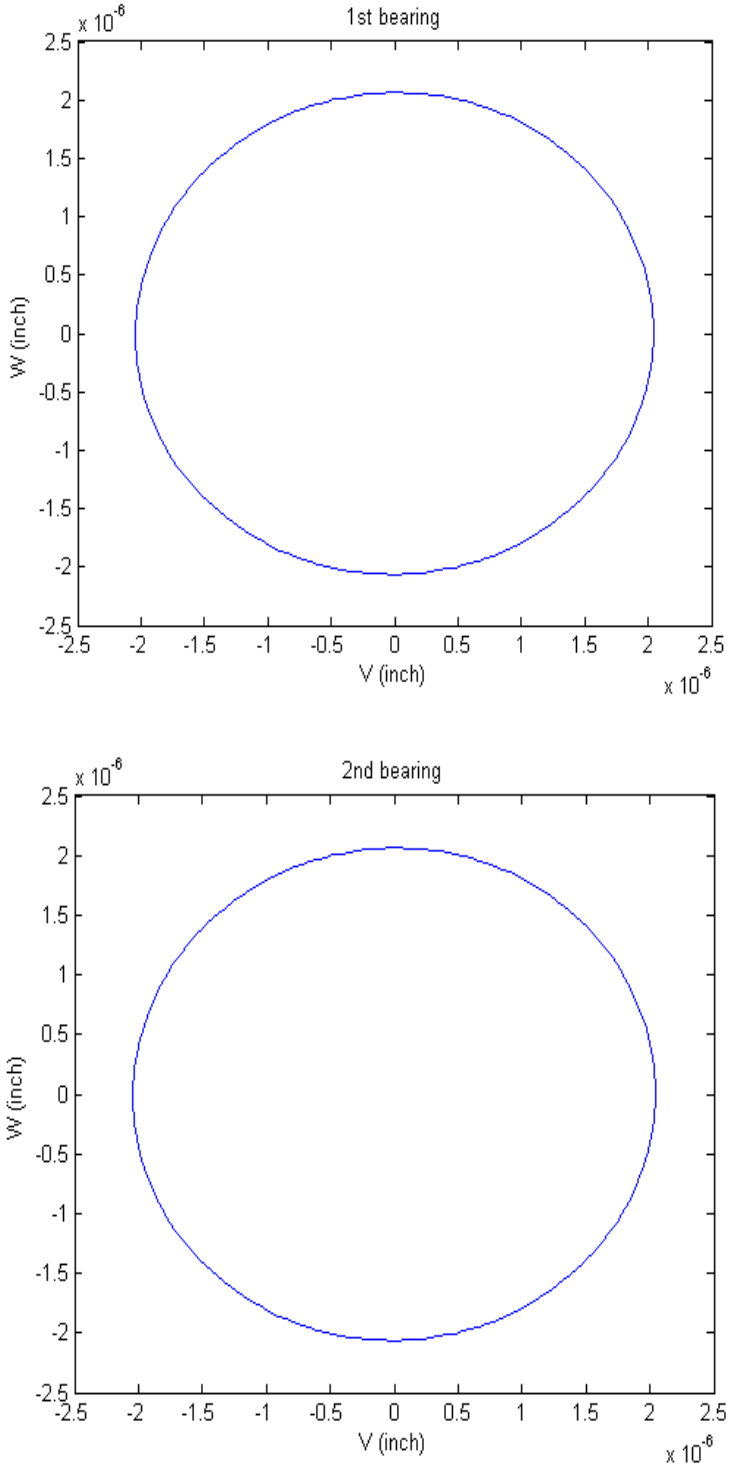

Figure 3-4. Rotor orbits at the two bearing supports at 1,000,000 rpm.

One of the most critical places is also tool end, next to the air turbine. Thus, rotor orbits should be found at tool end. As it can be seen from Figure 3-5, runout in both directions is small at the tool end (2×10^{-6} inch).

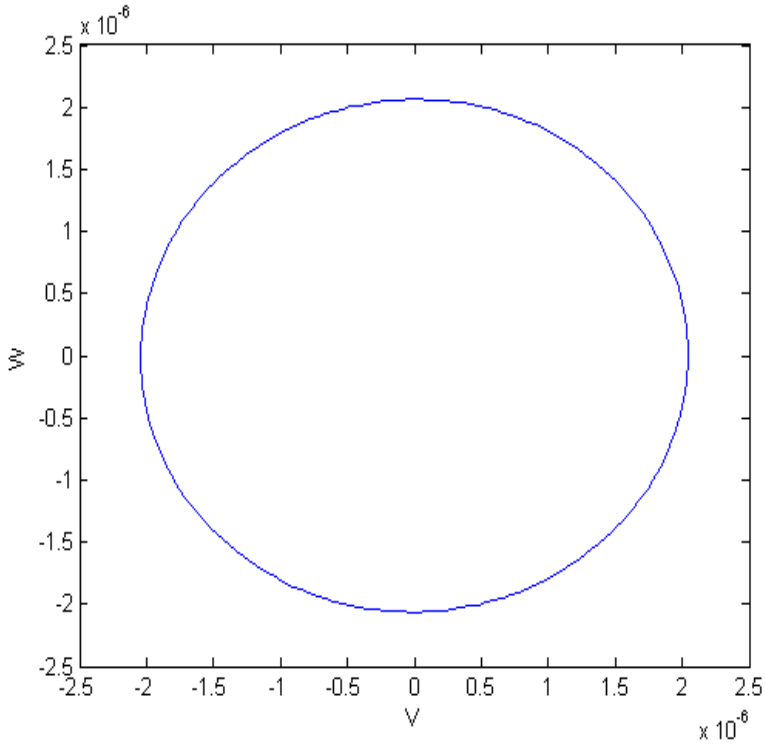

Figure 3-5. Rotor orbits at the tool end at 500,000 rpm.

The radial clearance was chosen 0.0002 inch. The eccentricity ratio ϵ will be 0.01 (ϵ=e/c) for the chosen unbalance.

Figure 3-6 shows that why figure 3-3 and figure 3-4 is same. It can be seen that after 500,000 rpm runout is nearly same and it is 2×10^{-6} inch. In addition this figure shows that highest amplitude is between 100,000 rpm and 120,000 rpm. Later, it will be shown that the rigid body critical speeds are 105,042 rpm and 115,231 rpm.

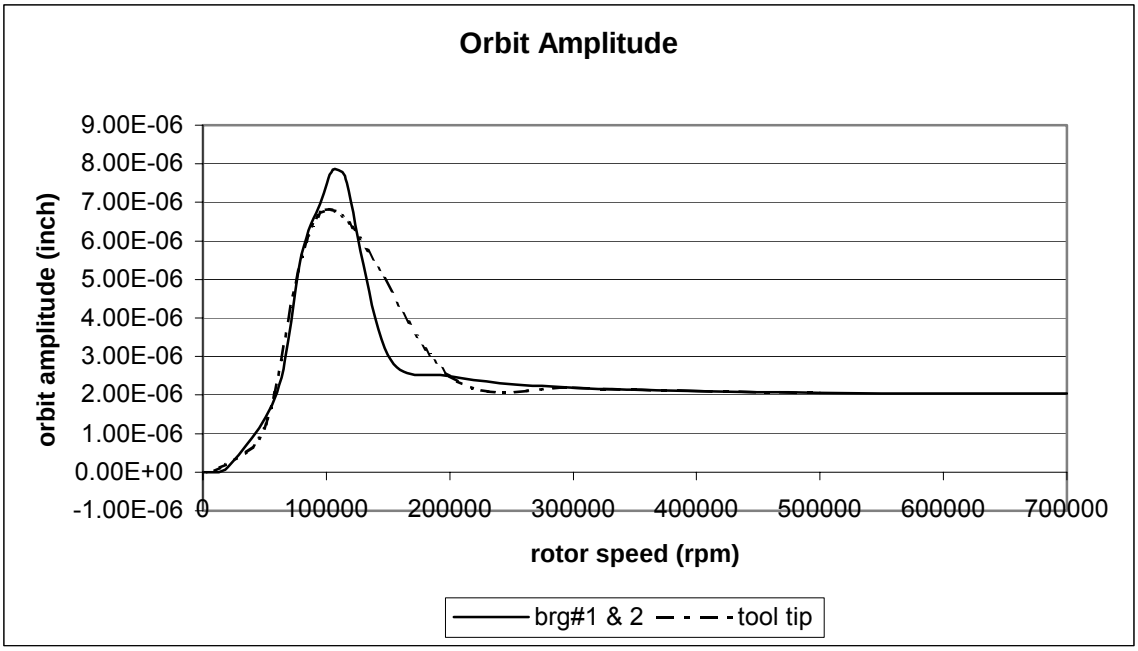

Figure 3-6. Orbit amplitude at 1st, 2nd bearing and tool tip.

Linear stability analysis has been performed based on energy dissipated at bearings. System is stable, if total energy dissipated is negative. Based on this criteria the system is stable over the entire speed range. For 500,000 rpm, total work (energy dissipated) per cycle at each bearing is found -4.24253×10^{-8} (see Appendix B).

Sample MathCAD program of rotor orbits can be found in Appendix B for a given spindle speed, 500,000rpm.

The bearing analysis code was coupled with the rotordynamics code in MATLAB, to efficiently explore the bearing/rotor design space. A direct interface to the bearing code used in XLTiltPadHGB was achieved by writing a MATLAB function. Input structures, viz: geometry, fluid, dynamic, operating, numerical were used to submit bearing parameters.

Thus the data plotting and visual inspection of bearing performance was facilitated by the MATLAB interface. This helped in the determination of factors that determine stiffness and damping. For example, stiffness as a function of the rotor eccentricity is

plotted in Figure 3-7. In this case, a constant gravity force was applied to the rotor and the bearing contained four pads.

The bearing stiffness and damping coefficients were passed from the bearing design code to the rotordynamic code. These coefficients are influenced by the bearing design parameters, and influence the rotordynamics. The rotor orbits within the bearings are calculated using the rotordynamic model and these orbits and their characteristics determine the rotor performance.

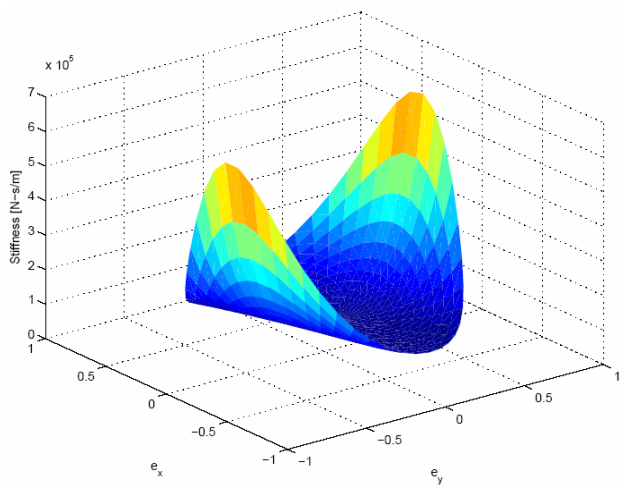

Figure 3-7. Stiffness, Kyy versus rotor eccentricity.

One of the most important aspects of research was to analyze rotor performance at critical speeds. Thus, rotor performance has been investigated at critical speeds. In order to find critical speeds, the following procedure has been adopted. It is known that eigenvalues can be found from equation with first order form. However equation of motion for rotor-bearing system is in second order. So equation (2-1) was modified in order to find eigenvalues.

$$\underline{M}\ddot{\bar{q}} + (\underline{C} - \Omega\underline{G})\dot{\bar{q}} + \underline{K}\bar{q} = \bar{Q} \tag{2-1}$$

$$\underline{M}^* = \begin{bmatrix} 0 & \underline{M} \\ \underline{M} & \underline{C} \end{bmatrix} \qquad \underline{K}^* = \begin{bmatrix} -\underline{M} & 0 \\ 0 & \underline{K} \end{bmatrix}$$

$$\bar{x} = \begin{Bmatrix} \dot{\bar{q}} \\ \bar{q} \end{Bmatrix} \qquad \bar{X} = \begin{Bmatrix} \bar{Q} \\ 0 \end{Bmatrix} \tag{3-5}$$

After entering equations (3-5) into (2-1), results in:

$$\underline{M}^{*}\dot{\bar{x}} + \underline{K}^{*}\bar{x} = \bar{X} \tag{3-6}$$

In order to find eigenvalues, right hand side of equation (3-6) is set to zero, and a harmonic solution $\bar{x} = e^{j\omega t}$ and $\dot{\bar{x}} = j\omega e^{j\omega t}$ is assumed. After rearranging equation (3-6), the standard E.V.P (eigenvalue problem) of the term $\underline{A}\bar{x} = \lambda\bar{x}$ can be set up, as shown below:

$$(-j\underline{K}^{*-1}\underline{M}^{*})\bar{x}_0 = \lambda\bar{x}_0 \qquad \text{where} \quad \lambda = \frac{1}{\omega} \tag{3-7}$$

In order to find all eight eigenvalues (four of which are complex conjugates of the other four) for a given spindle speed, a MathCAD program was generated to solve expression obtained above. The rotor whirl map was finally generated using these eigenvalues.

The whirl map for a rotor with a mass=2.525x10^{-4} lbf-sec^2/in, Ip=4.187x10^{-6} lbf-sec^2-in, Id=4.894x10^{-8} lbf-sec^2-in and an unbalance eccentricity of 0.000002 inch is shown in Figure 3-12; wherein the air bearing has the following parameters, Table 3-2.

Table 3-2. Bearing Parameters for different rotor speeds.

Kyy1,2	Kyz1,2	Kzy1,2	Kzz1,2	[lbf/in]	Ω	[rad/sec]
1069.2	99.1	-67.52	1069.2		62831	
950.4	99.1	-93.46	1050.4		52000	
831.6	105.04	-109.4	831.6		42000	
751.9	115.92	-151.28	751.9		32000	
700.8	118.8	-118.8	700.8		22000	
623.4	178.2	-115.8	623.4		12000	
594	190.08	-91.28	594		9500	
159.2	137.22	-85.34	159.2		2000	

Table 3-2. Continued

Kyy1,2	Kyz1,2	Kzy1,2	Kzz1,2	[lbf/in]	Ω	[rad/sec]
36.7	83.76	-53.76	36.7		500	

Cyy1,2	Cyz1,2	Czy1,2	Czz1,2	[lbf-sec/in]	Ω	[rad/sec]
0.015	-0.003	0.004	0.088		62831	
0.021	-0.004	0.005	0.106		52000	
0.033	-0.005	0.007	0.131		42000	
0.053	-0.009	0.01	0.158		32000	
0.086	-0.014	0.025	0.23		22000	
0.18	-0.042	0.077	0.383		12000	
0.287	-0.08	0.129	0.402		9500	
0.965	-0.011	0.018	0.322		2000	
1.838	-0.011	0.017	0.147		500	

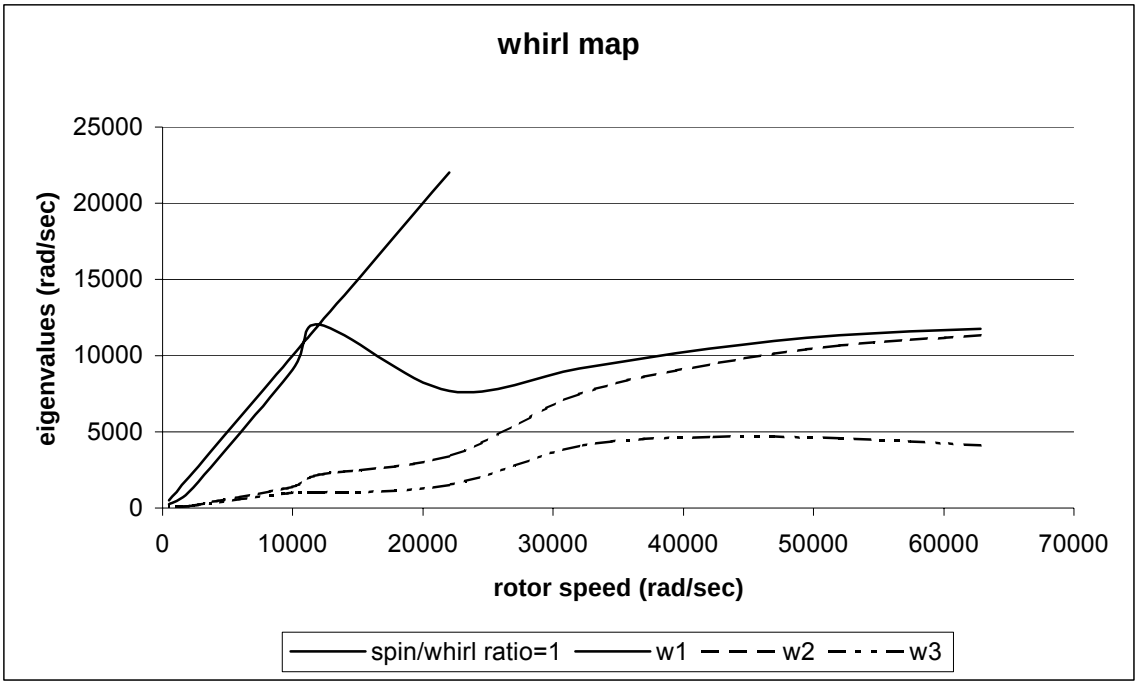

Figure 3-8. Whirl map.

It can be seen from graph (Figure3-8), critical speeds are 11000 rad/sec (105,042 rpm) and 12067 rad/sec (115,231 rpm).

MathCAD program for different air bearing stiffness and damping values, found by using XLTiltPadHGB, can be found in Appendix C.

3.2 Finite Element Analysis

The rotordynamics analysis of the rotor-bearing system was performed using a special-purpose code. The model shown in Figure 3-9 has 10 finite elements, 11 nodes, with each node having 4 degrees of freedom. The rigid body and flexural natural frequencies and model shapes can be computed from this model. To use finite element method it is assumed stiffness coefficient fixed and no cross coupling stiffness. The model parameters are bearing stiffness = 1,000 lb/in (fixed), bearing span = 0.5 in, shaft dia = 0.125 in, shaft length = 0.925 in and the shaft material is tungsten carbide. In addition, $me_u = 10^{-6}$ oz-in is used in FE model. As a result four critical speeds are found for the following parameters.

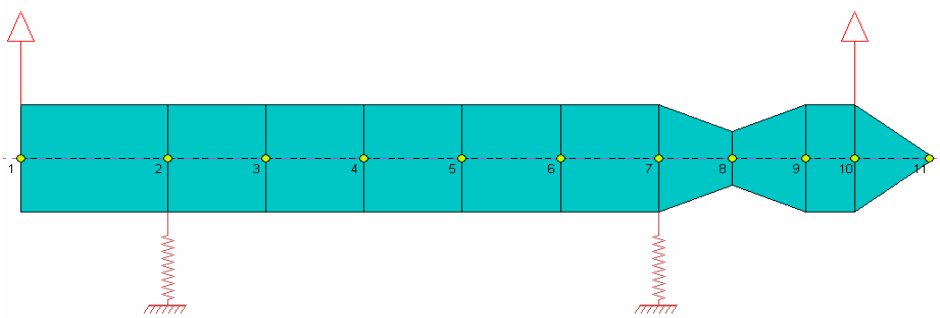

Figure 3-9. Finite element model.

The rigid body critical speeds are 107,758, 115,298, while the flexural critical speeds are 2,042,349 and 4,955,776 rpm.

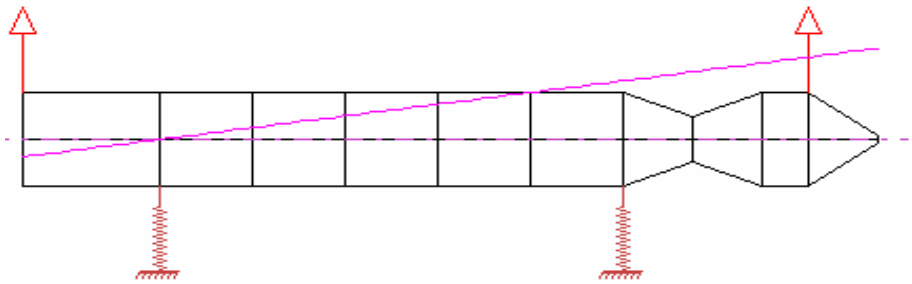

Figure 3-10. Rigid body mode 1, 107758 rpm.

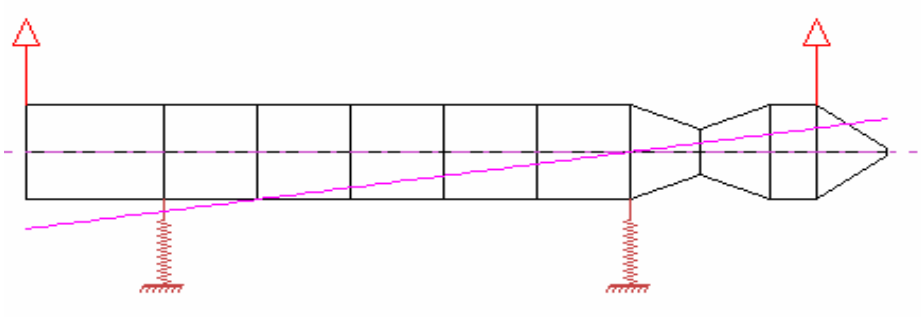

A.

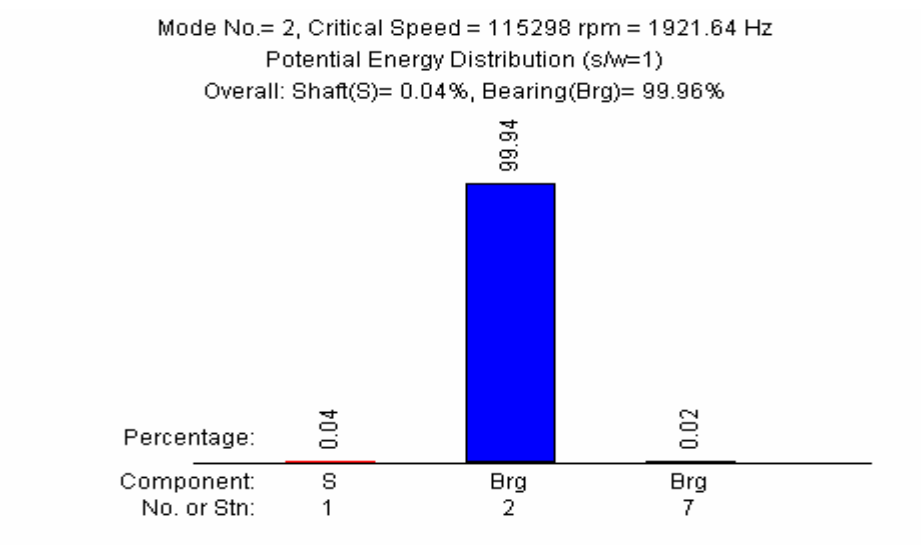

B.

Figure 3-11. Rotor analysis at 115298 rpm. A) Rigid body mode 2, B) Potential energy distribution.

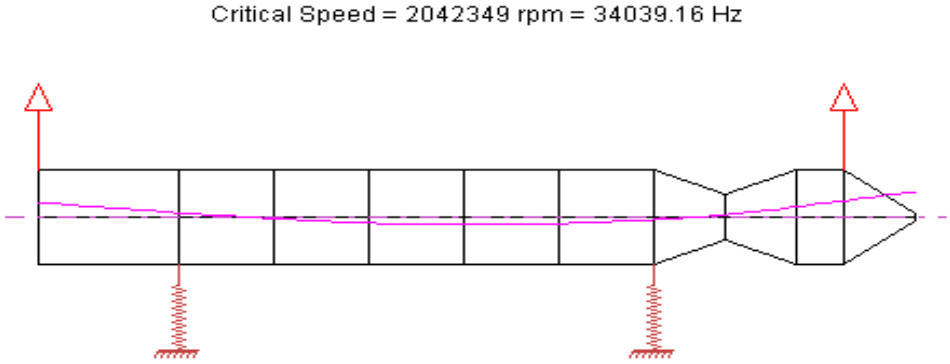

A.

Figure 3-12. Rotor analysis at 2,042,349 rpm. A) Flexural mode 1, B) potential energy distribution.

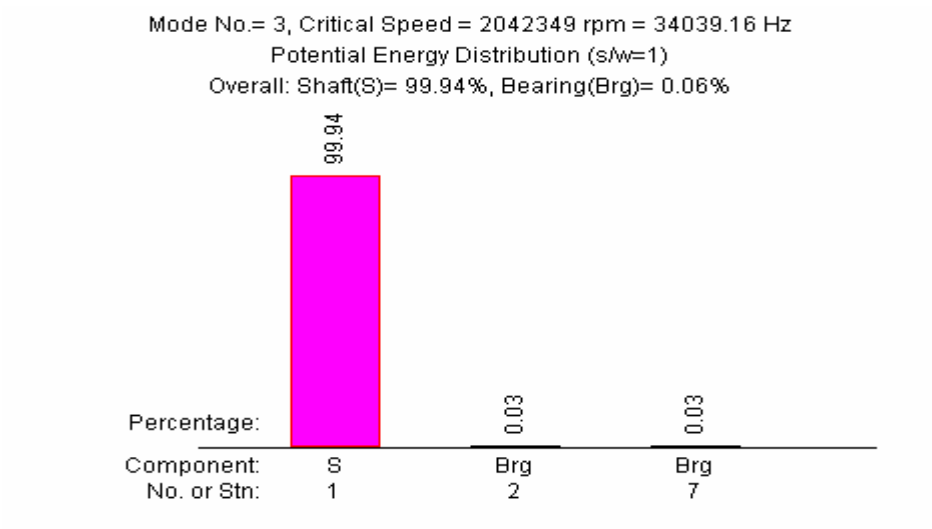

B.

Figure 3-15. Continued

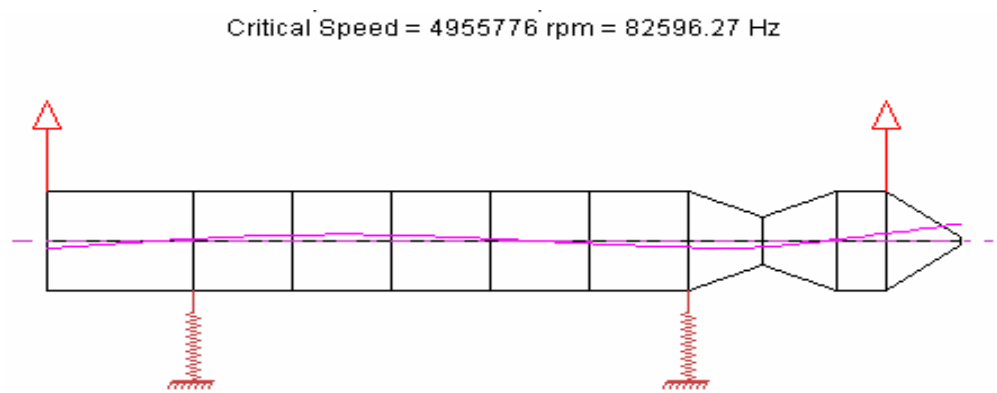

Figure 3-13. Flexural mode 2, 4,955,776 rpm.

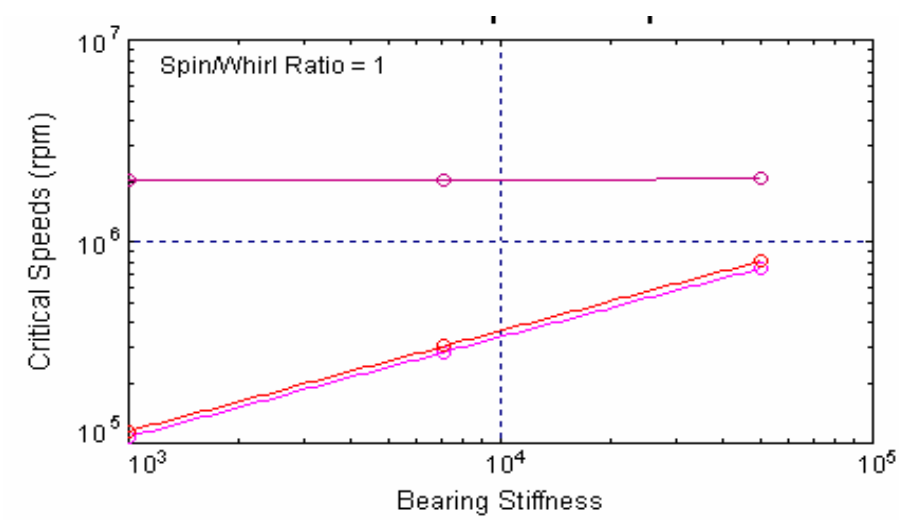

Figure 3-14. Critical speed map.

The critical speed map in Figure 3-14 shows that the flexural modes are unaffected by bearing stiffness, while the two rigid body modes increase with bearing stiffness.

There are three critical points on the tool such as; two bearing positions and tool tip. As a result the following analysis are found for these positions.

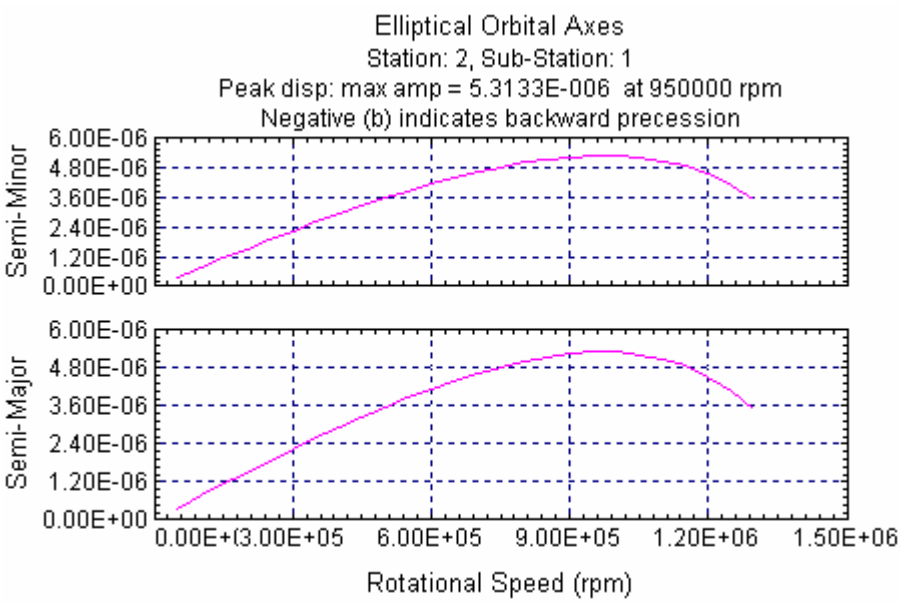

A.

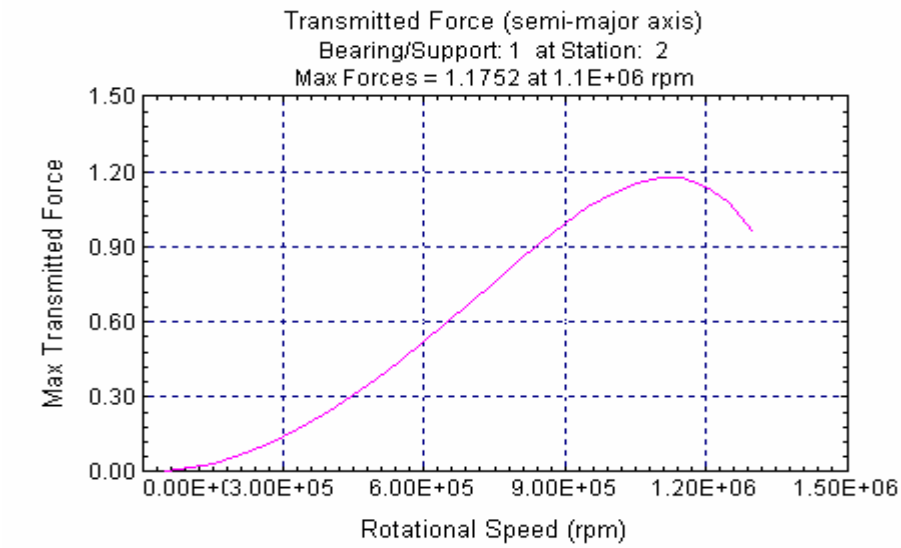

B.

Figure 3-15. 1st bearing. A) and B) Unbalance response, C) Amplitude and phase lag, D) Nyquist plot for displacement.

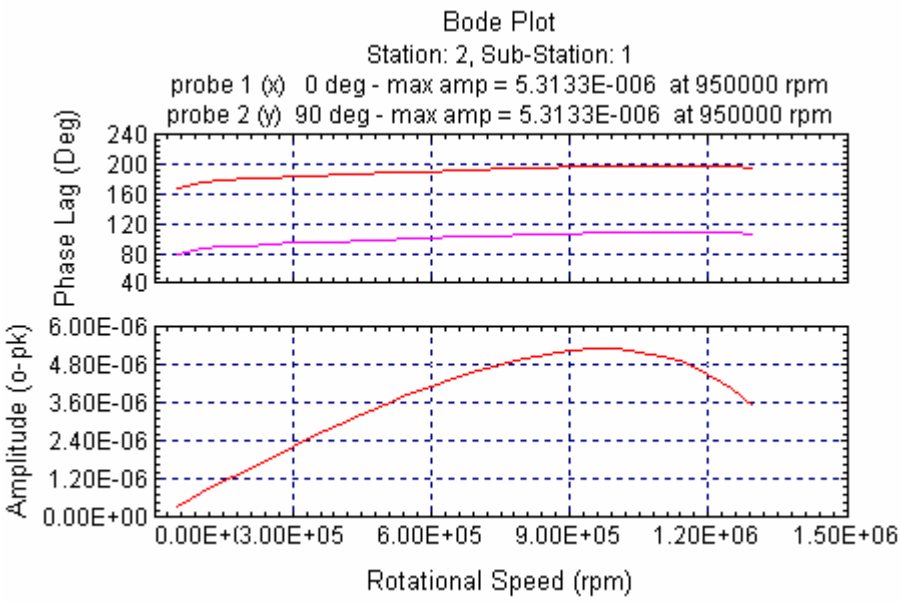

C.

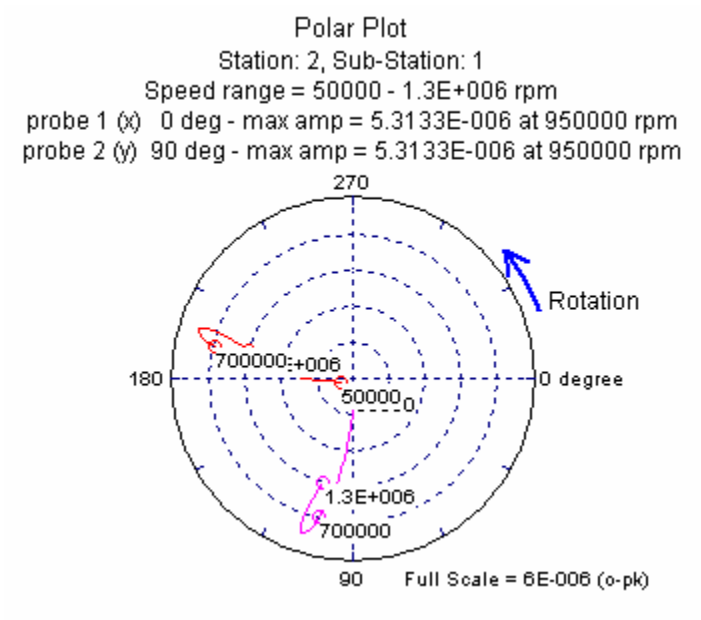

D.

Figure 3-15. Continued

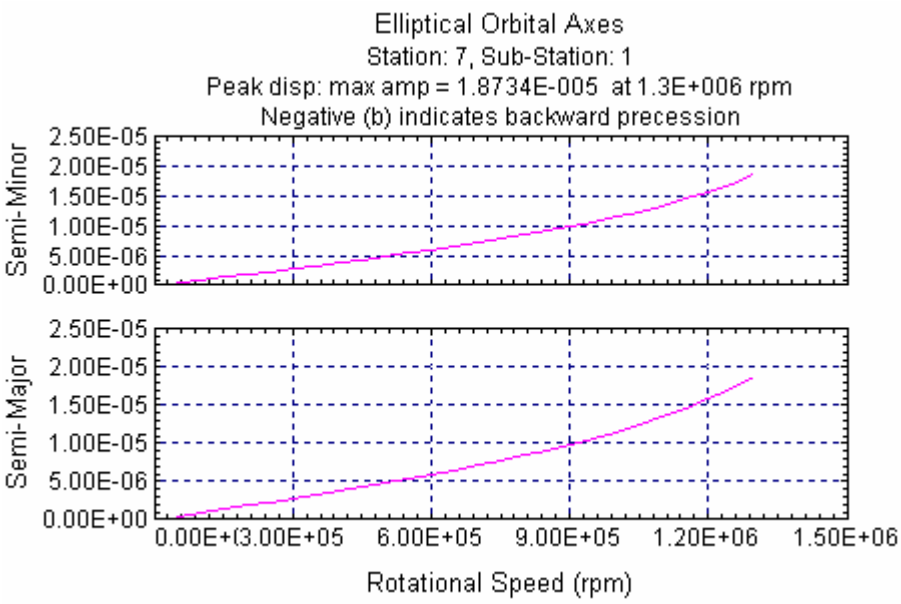

A.

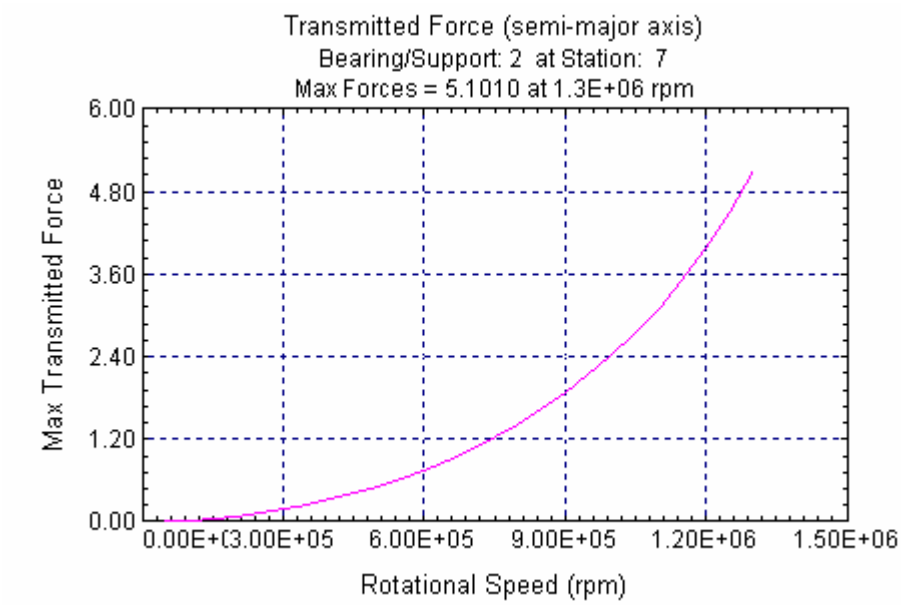

B.

Figure 3-16. 2nd bearing. A) and B) Unbalance response, C) Amplitude and phase lag, D) Nyquist plot for displacement.

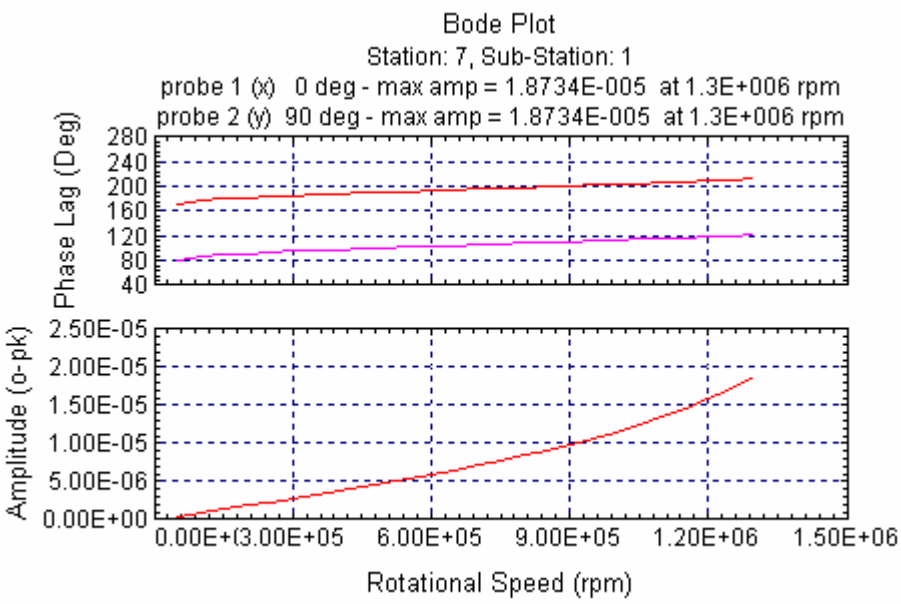

C.

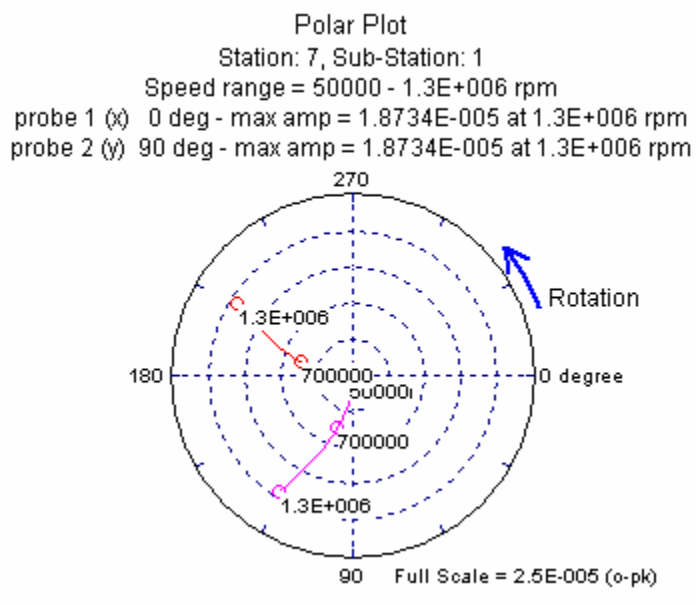

D.

Figure 3-16. Continued

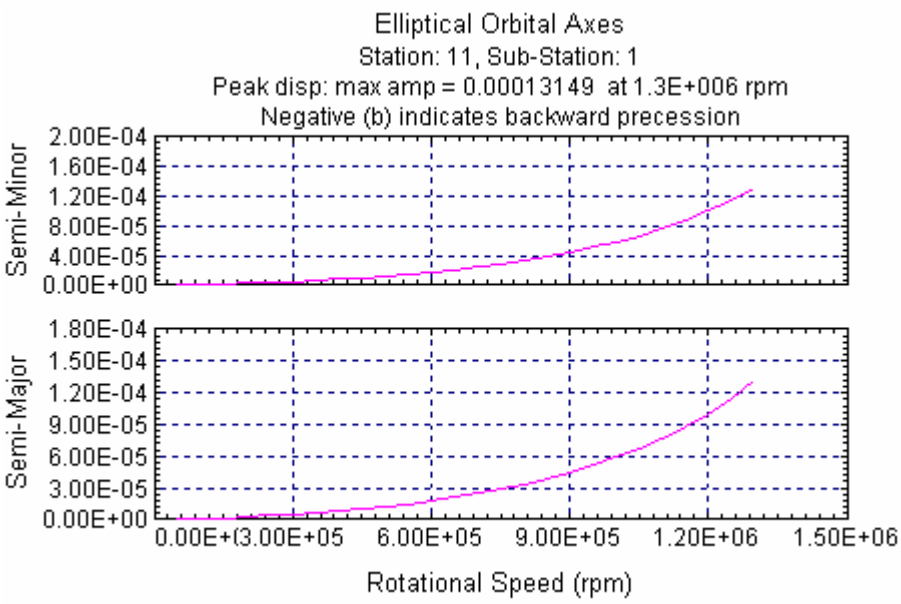

A.

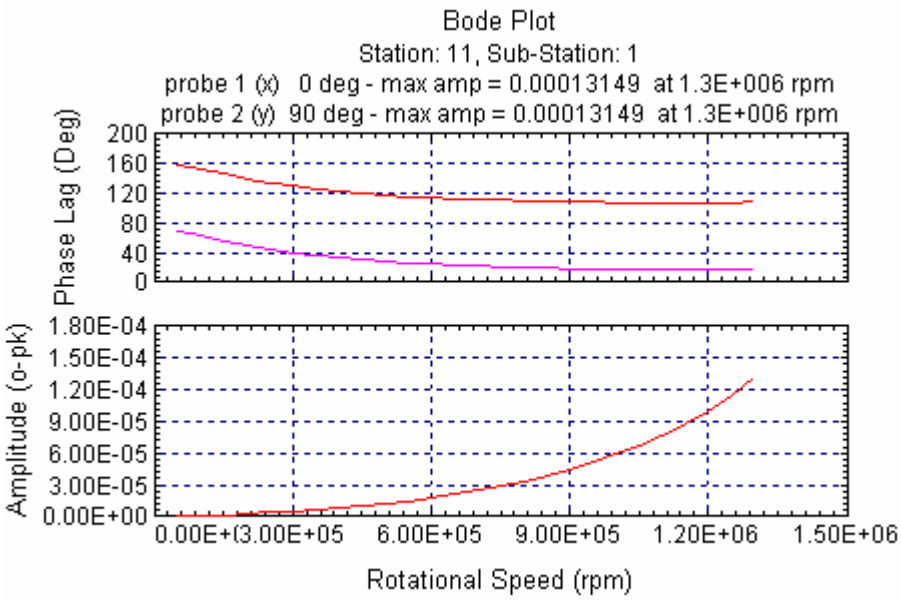

B.

Figure 3-17. Tool tip. A) Unbalance response, B) Amplitude and phase lag, C) Nyquist plot for displacement.

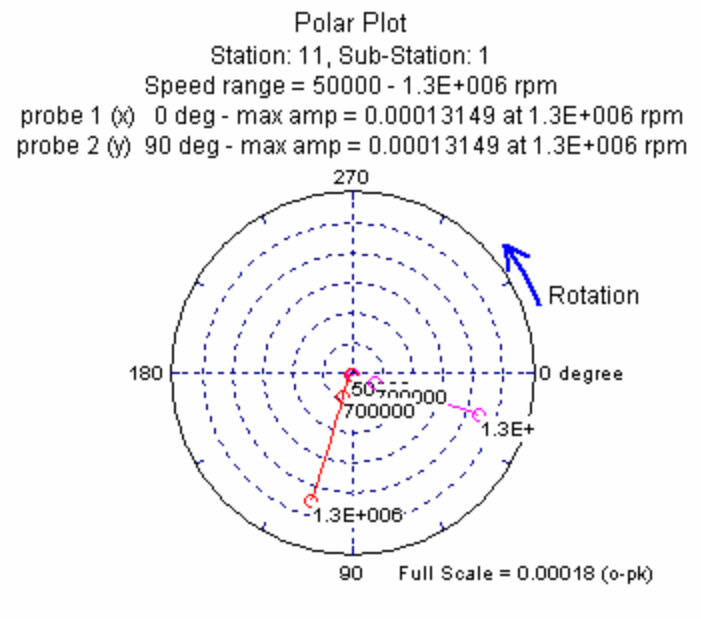

C.

Figure 3-17. Continued

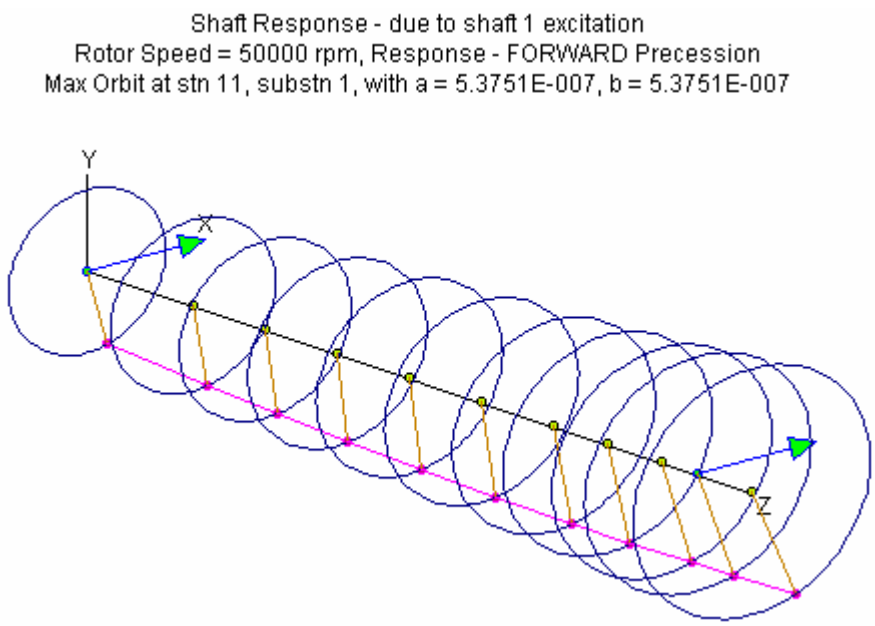

A.

Figure 3-18. Shaft orbits. A), B), C), D), E), F) are shaft orbits as a function of speed.

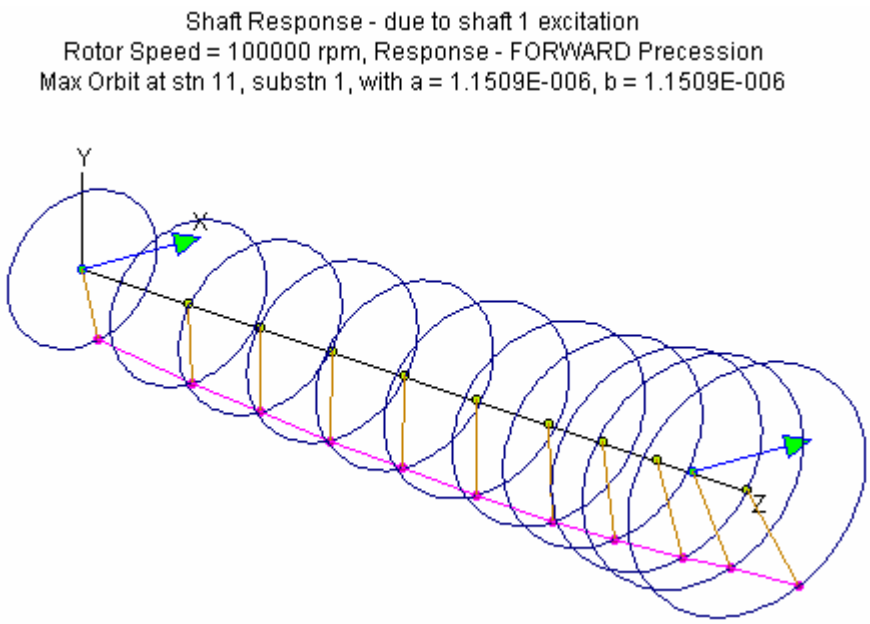

B.

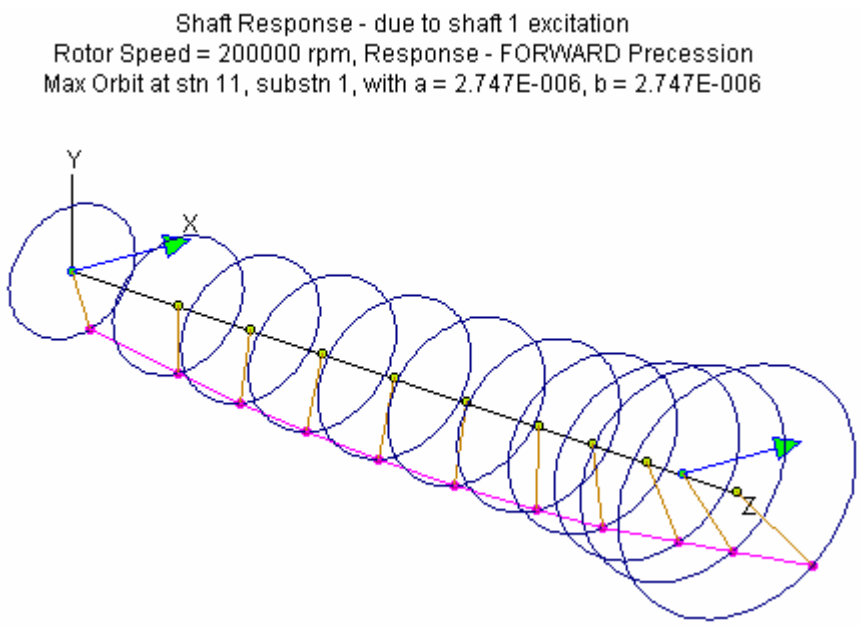

C.

Figure 3-18. Continued

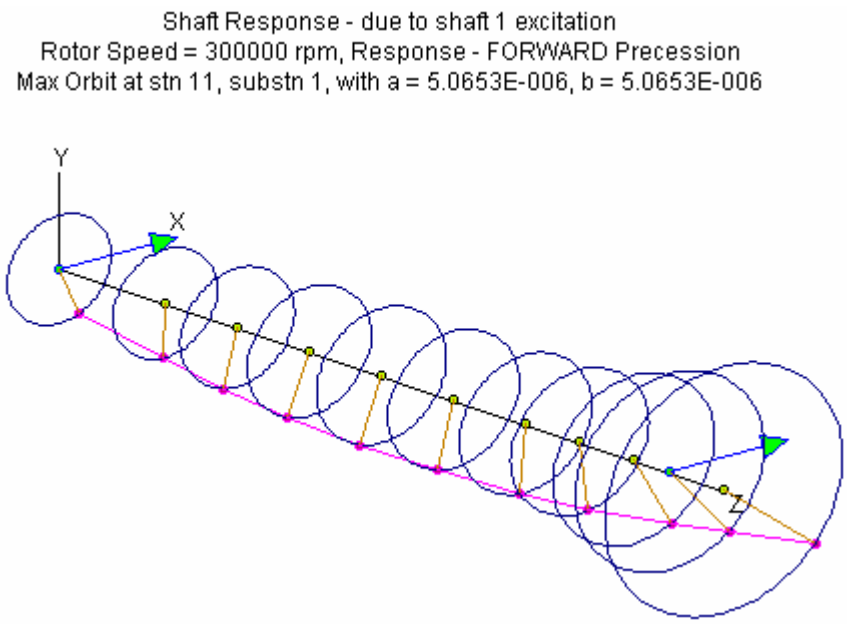

D.

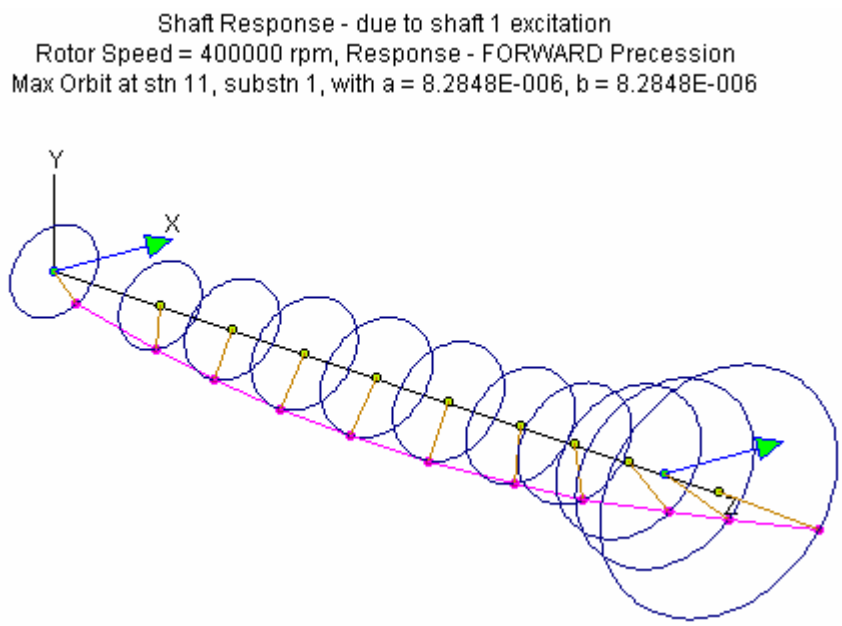

E.

Figure 3-18. Continued

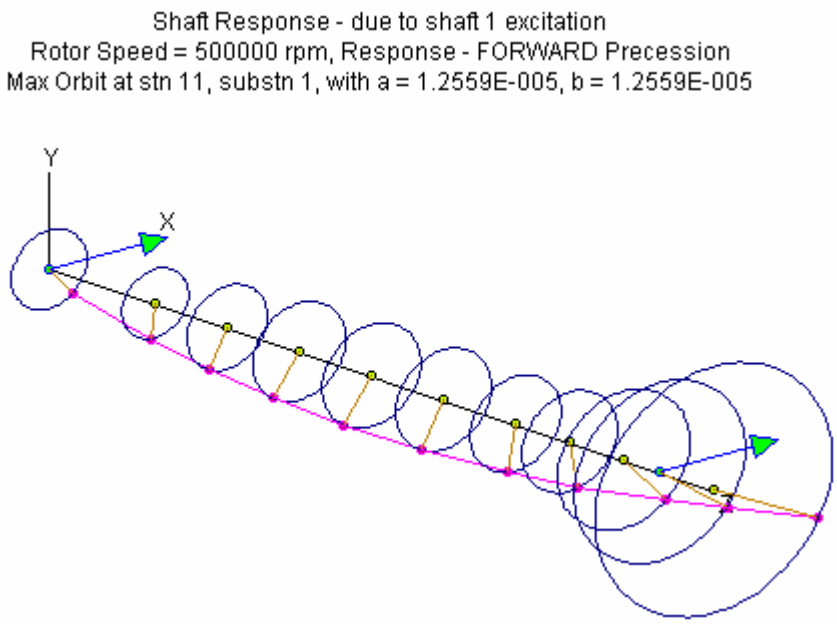

F.

Figure 3-18. Continued.

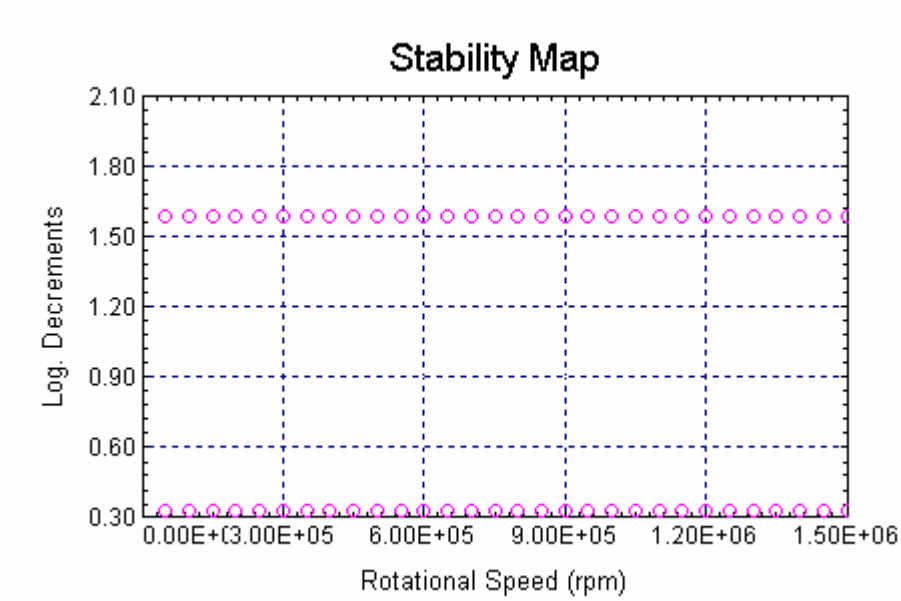

Figure 3-19. Stability Map (Note: Negative log decrements indicate instability).

3.3 Summary

Rigid body critical speeds (107,758 and 115,298 rpm) found by FEA are very close to the rotor analysis critical speeds (105,042 and 115,231 rpm) calculated by rigid rotor

analysis. The difference occurs, because in FEA analysis cross coupling stiffness terms and damping terms are eliminated and stiffness doesn't change with rotor speed.

For rigid rotor analysis eccentricity ratio is calculated ϵ=0.01, which can be questionable to get this value in practice, and it leads $m \times e_u = 1.22 \cdot 10^{-8}$ oz-in. So unbalance response analysis is performed again with ϵ=0.1. Figure 3-20 shows that even with this eccentricity ratio sub micrometer runout has been obtained for a given stiffness and damping parameters.

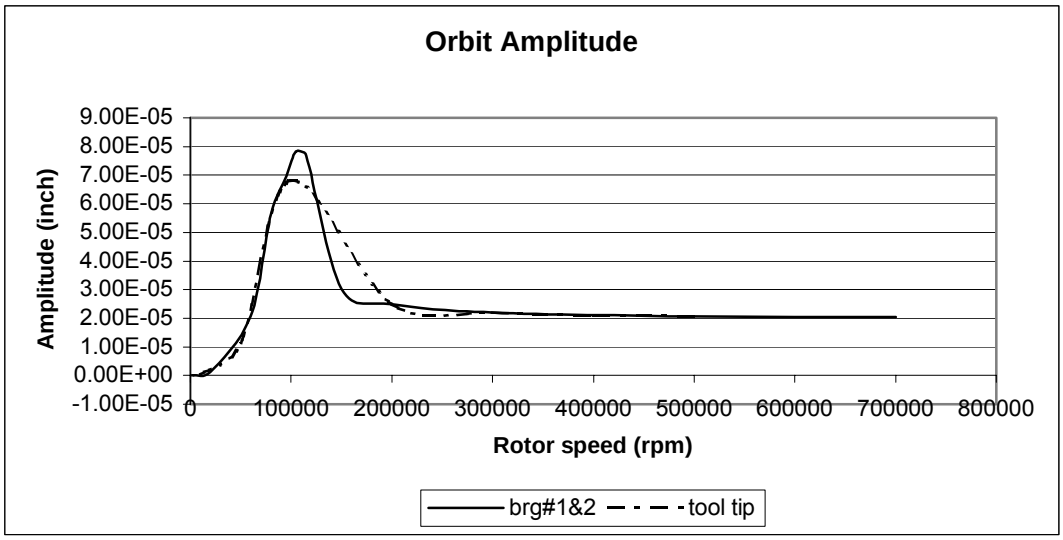

Figure 3-20. Orbit amplitude at 1st, 2nd bearing and tool tip, ϵ=0.1.

Both rigid rotor analysis (see appendix B) and FEA (see figure 3-19) shows system is stable.

CHAPTER 4
EXPERIMENTAL IDENTIFICATION OF BEARING PARAMETERS

In order to ensure proper operation, the vibration phenomena, which the rotors supported by fluid film bearings are especially subject to, has to be properly predicted. Knowledge of dynamic coefficients, stiffness and damping of a bearing prior to its installation and operation can be highly influential in the operation costs of the final machine. Both an analytical and experimental approach can be employed to study the dynamic behavior of bearings. Numerical techniques and computer-based simulation are usually used to perform analytical studies. The current research has used XlTiltPad program to identify bearing parameters.

The test set up aims at analyzing dynamic behavior of a tilted pad air bearing, which will be used in this research, and comparing the experimental results with analytical results. For the time being, experiments used a commercial air bearing as the tilted pad air bearing is in the process of being designed and for the initial studies; a flexure-supported ball bearing (see figure 4-1) is being used. Due to the difficulties found in exciting the rotor-bearing system and in the measurement of force and displacement data, experimental testing on fluid film bearings is known to be complex. The bearing parameters can be identified experimentally by six different methods as mentioned before. Since the research deals with a micro spindle supported by a small air bearing, the test setup will be also small making it extremely hard to use loading in order to excite the system. As a result, the viable way is using unbalance mass method.

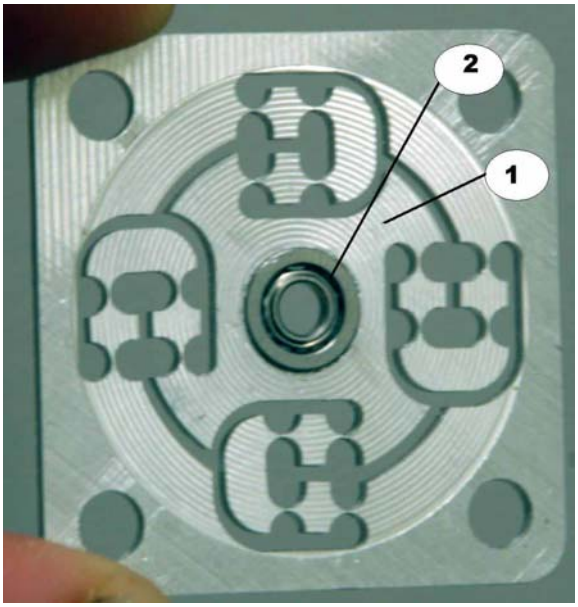

Figure 4-1. Flexure supported ball bearing: 1) Flexure, 2) Ball bearing.

4.1 Method of Measurement

The principle of operation of the test rig is rather simple: The bearing to be tested is placed on a chassis (see figure 4-2), which serves to support displacement probes and is mounted on dynamometer (load cell), used for measuring forces. A shaft is placed inside the bearing and one side of shaft is mounted to the high-speed spindle. Figure 4-3 shows a schematic of the test rig.

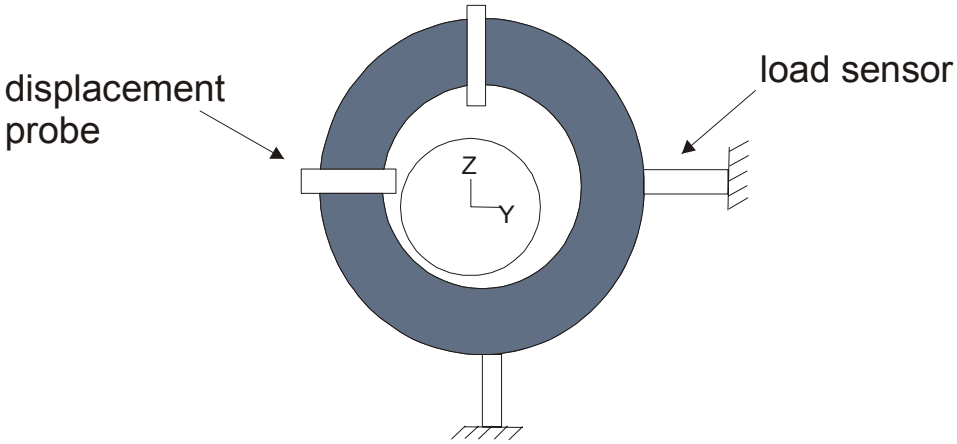

Figure 4-2. A chassis.

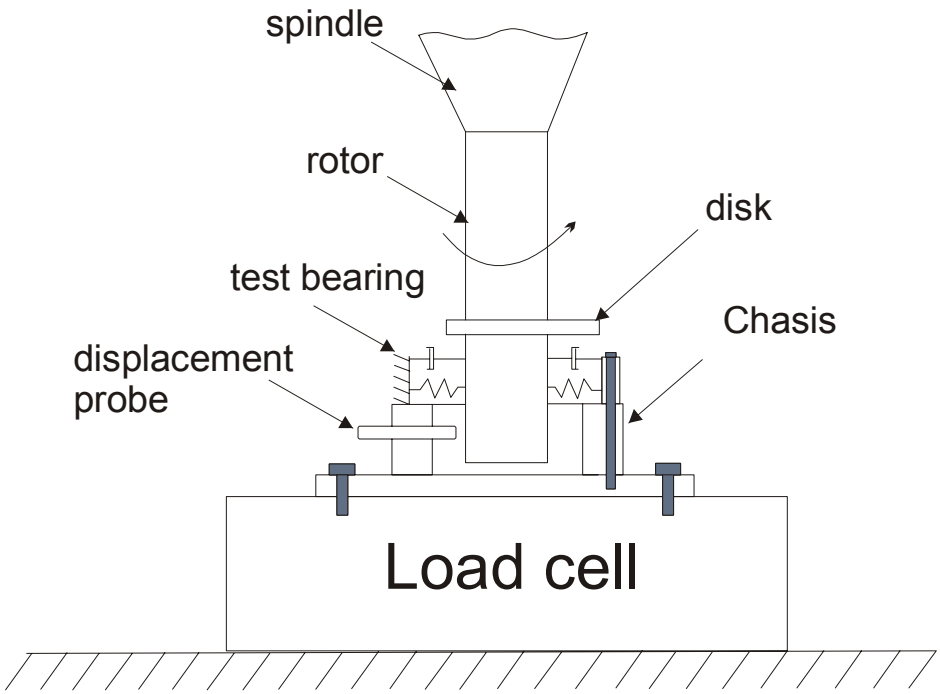

Figure 4-3. Schematic of the test rig.

The rotating part of the test bearing has been given an intentional eccentricity at the test bearing location. When the shaft rotates, the eccentricity generates an orbital pattern synchronous with shaft speed.

Since the shaft is driven with a synchronous harmonic load, the resulting shaft motion will, in general, be elliptic. Therefore, relative displacements describing ellipse as a function of time is in following form:

$$y(t) = a(\cos \omega t) + b(\sin \omega t) \tag{4-1}$$

$$z(t) = g(\cos \omega t) + h(\sin \omega t) \tag{4-2}$$

Following equations will be used in equation of motion:

$$\dot{y}(t) = -a\omega(\sin \omega t) + b\omega(\cos \omega t) \tag{4-1a}$$

$$\dot{z}(t) = -g\omega(\sin \omega t) + h\omega(\cos \omega t) \tag{4-2a}$$

The four coefficients a, b, g and h are termed Fourier coefficients, and ω is the tester speed in radians per second. They are obtained from the synchronous components of complex frequency spectrums computed for the y and z displacements.

The air bearing will respond with reaction forces which will be read by dyno to the off centered rotor movement. The same procedure applied to the load data which load cells read and following equations are derived:

$$F_y(t) = m(\cos \omega t) + n(\sin \omega t) \tag{4-3}$$

$$F_z(t) = p(\cos \omega t) + q(\sin \omega t) \tag{4-4}$$

Equation of motion is the following:

$$\begin{pmatrix} F_y \\ F_z \end{pmatrix} = \begin{pmatrix} K_{yy} & K_{yz} \\ K_{zy} & K_{zz} \end{pmatrix} \begin{pmatrix} y \\ z \end{pmatrix} + \begin{pmatrix} C_{yy} & C_{yz} \\ C_{zy} & C_{zz} \end{pmatrix} \begin{pmatrix} \dot{y} \\ \dot{z} \end{pmatrix} + \begin{pmatrix} M_{yy} & M_{yz} \\ M_{zy} & M_{zz} \end{pmatrix} \begin{pmatrix} \ddot{y} \\ \ddot{z} \end{pmatrix} \tag{4-5}$$

Inertia term can be neglected in equation, because shaft relative displacement is so small that inertia force will not contribute a lot for air film force. So new equation is the following:

$$\begin{pmatrix} F_y \\ F_z \end{pmatrix} = \begin{pmatrix} K_{yy} & K_{yz} \\ K_{zy} & K_{zz} \end{pmatrix} \begin{pmatrix} y \\ z \end{pmatrix} + \begin{pmatrix} C_{yy} & C_{yz} \\ C_{zy} & C_{zz} \end{pmatrix} \begin{pmatrix} \dot{y} \\ \dot{z} \end{pmatrix} \tag{4-6}$$

After substituting (4-1), (4-2), (4-1a), (4-2a), (4-3) and (4-4) into (4-6), the following equation is obtained:

$$\begin{pmatrix} b\omega & h\omega & a & g & 0 & 0 & 0 & 0 \\ -a\omega & -g\omega & b & h & 0 & 0 & 0 & 0 \\ 0 & 0 & 0 & 0 & b\omega & h\omega & a & g \\ 0 & 0 & 0 & 0 & -a\omega & -g\omega & b & h \end{pmatrix} \begin{Bmatrix} C_{yy} \\ C_{yz} \\ K_{yy} \\ K_{yz} \\ C_{zy} \\ C_{zz} \\ K_{zy} \\ K_{zz} \end{Bmatrix} = \begin{Bmatrix} m \\ n \\ p \\ q \end{Bmatrix} \tag{4-7}$$

Since all these bearing parameters are functions of speed, it is necessary that the speeds span as wide a range as possible to give the best definition of the coefficients [16]. There is an example how to use equation (4-7) in Appendix D.

4.2 Design Process

The test rig was designed and developed relying on an existing dynamometer, as seen in Figure 4-4. Detailed information about dynamometer is presented in Appendix E. In order to facilitate a better understanding of the setup, it was divided in to four parts that is the dyno; a main chassis (see Figure 4-5), which serves to mount displacement probes in order to measure shaft displacement and to mount the test bearing; a shaft; and a spindle, which is an electric driven motor and rotates at 50000 rpm (max.).

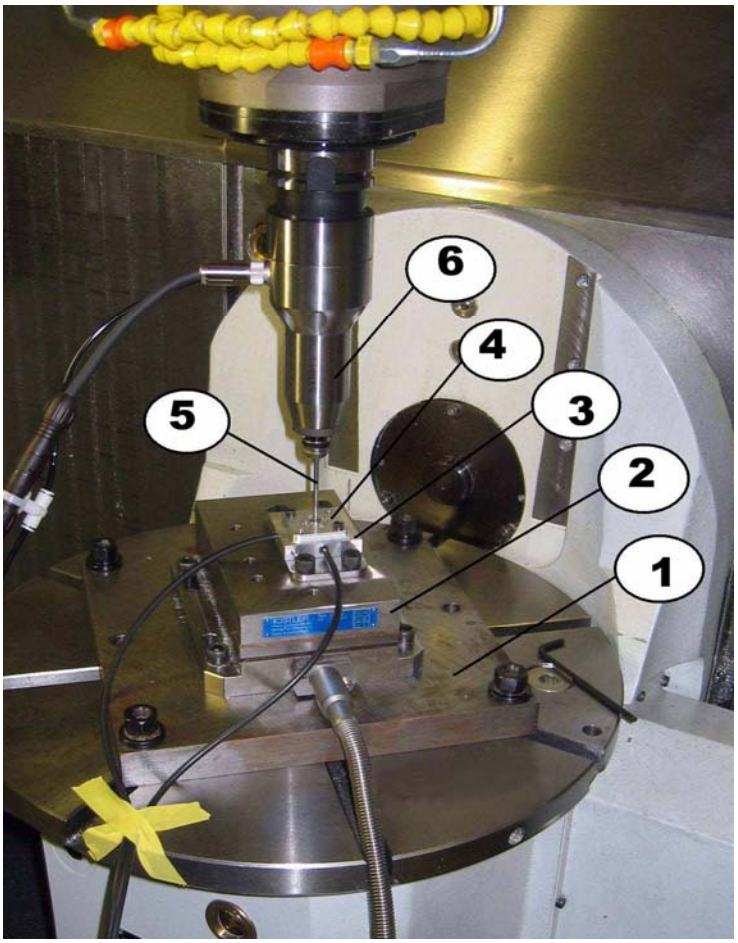

Figure 4-4. Test Setup: 1) Base, 2) Dyno, 3) Chassis, 4) Test bearing, 5) Shaft, 6) Spindle

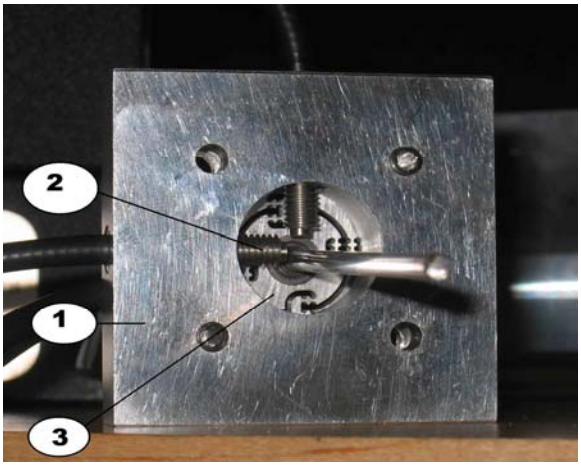

Figure 4-5. Main Chassis: 1) Stator, 2) Displacement Probe, 3) Test Bearing.

The shaft motion is determined by displacement probes, and results can be read on PC by using fiber optic sensors (RC20) connected to the PC. Dyno is used to measure the forces in x and y directions respectively, and the data is sent to the PC using a charge amplifier. A NSK spindle drive controller adjusts the spindle speed. The complete measurement system is illustrated in Figure 4-6.

Figure 4-6. Measurment system

CHAPTER 5
CONCLUSION AND RECOMMENDATIONS

The current research provides initial results for the development of a comprehensive rotordynamics analysis to describe high-speed micro spindle vibrations. Results demonstrate that the air bearing characteristics and spindle residual unbalance levels dictate the critical speed placement, unbalance response, and the ability to limit the tool tip runout to sub-micrometer levels.

Results demonstrate that the 1/8th inch tungsten carbide micro spindle with the integrally machined air turbine at one end and the end mill cutter at the other end can indeed operate with sub-micrometer runout at the tool tip for spindle speeds up to 1 million rpm. Air bearing stiffness used is about 2000 lb/in. Spindle residual unbalance level assumed is 10^{-6} oz-in (me=. 000001 oz-in). Residual unbalance two to three times this level will also be adequate with higher bearing stiffness. Turbine engine shafts weighing 100 lbs or greater are routinely balanced to 0.1 oz-in. Considering that the end mill cutter weighs about 0.07 lb, the recommended unbalance limits can be achieved in practice.

Next step in this research is experimental analysis, which was undertaken to understand behavior of the air bearing. Since the air bearing is yet to be fabricated, a simple test rig has been built to test the spindle mounted on ball bearings with a flexure support. The x-y displacements at the bearings, as a function of speed, are being used to evaluate the support stiffness characteristics. Our goals are to demonstrate the feasibility of the proposed parameter estimation scheme to evaluate support stiffness.

APPENDIX A
CHRONOLOGICAL LIST OF PAPERS ON THE EXPERIMENTAL DYNAMIC PARAMETER IDENTIFICATION OF BEARINGS

References	Bearing type*	Type of excitation	Vibration response measured	Identified dynamic parameters
Hagg and Sankey (1956, 1958)	HDJ	Unbalance	Displ. (frequency)	Direct damping and stiffness
Mitchell et al. (1965–66)	HDJ	Incremental static load	Displacement	Stiffness
Duffin and Johnson (1966–67)	HDJ	Unbalance	Displ. (frequency)	Direct damping and stiffness
Glienicke (1966–67)	HDJ	Sinusoidal	Displ. (frequency)	Damping and stiffness
Woodcock and Holmes (1969–70)	HDJ	Unbalance	Displ. (frequency)	Damping and uncertainty
Black and Jenssen (1969–70)	PLS	Incremental static load	Displacement	Stiffness
Morton (1971)	HDJ	Sinusoidal	Displ. (frequency)	Damping and stiffness
Williams and Holmes (1971)	SQF	Static load	Ecc., alt., angle, vel.	Damping
Thomsen and Andersen (1974)	SQF	Unbalance	Displ. (frequency)	Damping
Morton (1975a)	HDJ	Step function	Displ. (frequency)	Damping and stiffness
Bannister (1976)	HDJ	Unbalance	Displ. (frequency)	Damping, stiffness and 28 non-linear coefficients
Tonnesen (1976)	SQF	Unbalance	Displ. (frequency)	Damping
Fleming et al. (1977)	GJ	Unbalance	Displ. (frequency)	Damping and stiffness
Wright (1978)	LS	Impact	Displ. (time)	Damping and stiffness
Parkins (1979)	HSJ	Bi-directional sine	Displ., vel. (time)	Damping and stiffness
Stanway et al. (1979a, 1979b)	SQF	PRBS	Displ. (time)	Damping
Childs et al. (1980)	Seals	Eccentric shaft	Displ. (frequency)	Mass, damping and stiffness
Diana et al. (1980)	HSJ	Inertial exciter	Displ. (frequency)	Damping and stiffness
Dogan et al. (1980)	HDJ	PRBS	Displ. (frequency)	Damping and stiffness
Hisa et al. (1980)	HDJ	Sinusoidal	Vel. (frequency)	Damping and stiffness
Iino and Kaneko (1980)	PLS	Synchronous	Displ. (frequency)	Mass, damping and stiffness
Nordmann and Schöllhorn (1980)	HDJ	Impact	Displ. (frequency)	Damping and stiffness
Walford and Stone (1980a, 1980b)	Ball	Sinusoidal	Displ., acc. (frequency)	Damping and stiffness
Burrows et al. (1981)	SQF	PRBS/SPHS	Displ. (frequency)	Damping
Parkins (1981)	HSJ	Bi-directional sine I	Displ., vel. (time)	Damping and stiffness
Burrows and Sahinkaya (1982a)	SQF	PRBS	Displ. (frequency)	Damping and uncertainty
Diana et al. (1982)	PLS	Synchronous	Displ. (frequency)	Stiffness
Stone (1982)	RE	Impact and Sine	Displ. (time, frequency)	Damping and stiffness
Goodwin et al. (1983)	HSJ	Unbalance	Displ. (frequency)	Damping and stiffness
Wright (1983)	GS	Synchronous	Displ. (frequency)	Damping and stiffness
Burrows et al. (1984)	SQF	SPHS	Displ. (frequency)	Damping
Falco et al. (1984)	PLS	Sinusoidal	Displ. (frequency)	Damping and stiffness
Goodwin et al. (1984)	HYJ	Unbalance	Displ. (frequency)	Damping and stiffness
Kanki and Kawakami (1984)	PLS	Sinusoidal	Displ. (frequency)	Mass, damping and stiffness
Nordmann and Massmann (1984)	ANS	Impact	Displ. (frequency)	Mass, damping and stiffness
Sahinkaya et al. (1984)	SQF	SPHS	Displ. (frequency)	Damping and uncertainty
Sahinkaya and Burrows (1984a)	SQF	SPHS	Displ. (time)	Damping and uncertainty
Burrows and Sahinkaya (1985)	SQF	SPHS	Displ., vel. (time, frequency)	Damping and uncertainty
Chang and Zheng (1985)	HDJ	Step function	Displ., acc. (frequency)	Damping and stiffness (0/4/4)
Childs and Kim (1985)	ALS	Eccentric rotor	Displ. (frequency)	Mass, damping and stiffness
Kaushal et al. (1985)	SQF	Unbalance	Displ. (frequency)	Damping (0/1/0) and uncertainty
Childs and Kim (1986)	DS	Eccentric rotor	Displ. (frequency)	Mass, damping and stiffness
Childs and Scharrer (1986)	GS	Sinusoidal	Displ. (frequency)	Damping and stiffness
Nelson et al. (1986)	ALS	Sinusoidal	Displ. (frequency)	Mass, damping and stiffness
Roberts et al. (1986)	SQF	Step function	Displ. (time)	Mass and damping
Childs and Garcia (1987)	DS	Eccentric rotor	Displ. (frequency)	Mass, damping and stiffness
Kraus et al. (1987)	Ball	Impact	Displ. (frequency)	Mass, damping and stiffness
Ramli et al. (1987)	SQF	Transient	Displ. (time)	Direct damping and stiffness
Stanway et al. (1987)	SQF	PRBS	Displ. (frequency)	Damping
Burrows et al. (1988a)	SQF	Unbalance	Displ. (frequency)	Mass and damping
Childs and Scharrer (1988)	LGS	Uni-directional sine	Displ. (frequency)	Damping, stiffness uncertainty
Ellis et al. (1988)	SQF	Step/sine	Displ. (time)	Direct damping and stiffness
Kang and Jin (1988)	HDJ	Impact	Displ., acc. (time)	Damping and stiffness (0/4/4)

References	Bearing type*	Type of excitation	Vibration response measured	Identified dynamic parameters
Roberts et al. (1988)	SQF	Sinusoidal	Displ. (frequency)	Mass, damping and stiffness
Stanway et al. (1988)	SQF	Synchronous	Displ. (frequency)	*n*th-power velocity damping
Childs et al. (1989)	HCS	Sine-sweep	Displ., acc. (frequency)	Damping, stiffness and uncertainty
Ellis et al. (1989)	SQF	Bi-directional sinel	Displ. (time)	Mass, damping and stiffness
Elrod et al. (1989)	HCS	Uni-directional sine	Displ. (frequency)	Damping, stiffness and uncertainty
Hawkins et al. (1989)	AGS	Uni-directional sinel	Displ., acc. (frequency)	Damping, stiffness and uncertainty
Kanemori and Iwatsubo (1989, 1992)	PLS	Eccentric rotor	Displ. (frequency)	Mass, damping and stiffness
Someya (1989)	HDJ	Sinusoidal	Displ. (frequency)	Damping and stiffness
Brockwell et al. (1990)	HDJ	Bi-directional sine	Displ. (frequency)	Damping and stiffness
Burrows et al. (1990)	SQF	SPHS	Displ. (frequency)	Mass, damping and uncertainty
Childs et al. (1990a)	HCS	Uni-directional sine	Displ., acc. (frequency)	Damping, stiffness and uncertainty
Childs et al. (1990b)	ANS	Eccentric rotor	Displ. (frequency)	Mass, damping and stiffness
Childs et al. (1990c)	DS	Eccentric rotor	Displ. (frequency)	Mass, damping and stiffness
Ellis et al. (1990)	SQF	Random	Displ. (time)	Mass, damping and stiffness
Fritzen and Seibold (1990)	ANS	Impact	Displ. (time)	Mass, damping and stiffness.
Iwatsubo and Sheng (1990)	DS	Eccentric sleeves	Displ. (frequency)	Mass, damping and stiffness
Kim et al. (1990)	TR	Impulse	Acc. (frequency)	Direct stiffness and damping
Kostrzewsky et al. (1990)	HDJ	Bi-directional sine	Displ. (frequency)	Stiffness and uncertainty
Matsumoto et al. (1990)	HDJ	Two-directional sine	Displ. (frequency)	Damping and stiffness
Mohammad and Burdess (1990)	HDJ	Random	Displ. (time)	Damping and stiffness
Muszynska and Bently (1990)	HDJ	Sine sweep	Displ. (frequency)	Damping and effective stiffness
Roberts et al. (1990)	SQF	Step function	Displ. (time)	Mass, damping and uncertainty
Rouch (1990)	SQF	Sinusoidal	Displ. (frequency)	Damping and stiffness
Yanabe et al. (1990)	HDJ	Incremental static/ unbalance/impact	Displacement (frequency)	Damping and stiffness
Chan and White (1991)	TPJ	Impact	Displ. (frequency)	Damping and stiffness
Childs and Ramsey (1991)	AGS	Sine sweep	Displ. (frequency)	Damping, stiffness and uncertainty
Childs et al. (1991)	AGS	Sine sweep	Displ. (frequency)	Damping, stiffness and uncertainty
Imlach et al. (1991)	MB	Incremental static load	Displacement	Direct stiffness
Jung et al. (1991a, 1991b)	SQF	Eccentric sleeve	Displ. (frequency)	Mass and damping
Murphy and Wagner (1991)	HSJ	Eccentric shaft	Displ. (frequency)	Damping, stiffness and uncertainty
Wang and Liou (1991)	Ball	Impact	Displ. (frequency)	Damping and stiffness
Adams et al. (1992)	HSJ	Unbalance	Displ. (frequency)	Mass, damping and stiffness
Brown and Ismail (1992, 1994)	ANS	Multi-frequency	Displ. (time)	Damping and stiffness
Childs and Kleynhans (1992)	ANS	Sine sweep	Displ. (frequency)	Damping, stiffness and uncertainty
Myllerup et al. (1992)	HDJ	Incremental static load	Displacement	Stiffness
Rouvas et al. (1992)	HSJ	Impact	Displ., acc. (frequency)	Mass, damping and stiffness
Sakakida et al. (1992)	HSJ	Sinusoidal	Displ., acc. (frequency)	Damping and stiffness
Zhang et al. (1992a, 1992b)	HDJ	Impact	Displ. (frequency)	Damping, stiffness and uncertainty
Conner and Childs (1993)	BS	Sine-sweep	Displ. (frequency)	Damping, stiffness and uncertainty
Flack et al. (1993)	HDJ	Bi-directional sine l	Displ. (frequency)	Damping, stiffness, uncertainty
Jung and Vance (1993)	SQF	Eccentric sleeve	Displ. (frequency)	Mass and damping
Muszynska et al. (1993)	Seals	Unbalance	Displ. (frequency)	Radial damping and stiffness
Parkins and Horner (1993)	HDJ	Incremental static load	Displacement	Stiffness
Roberts et al. (1993)	SQF	Sinusoidal	Displacement (time)	Non-linear model
Rouvas and Childs (1993)	HSJ	PRBS and Sine	Displ., acc. (frequency)	Mass, damping and stiffness
Childs and Hale (1994)	HSJ	PRBS	Displ., acc. (frequency)	Mass, damping and stiffness
Franchek and Childs (1994)	HYJ	PRBS	Displ., acc. (frequency)	Mass, damping and stiffness
Heshmat and Ku (1994)	HDJ (foil)	Sinusoidal	Displ., acc. (frequency)	Damping, stiffness and uncertainty
Kim and Lee (1994)	Seals	Impact	Displ. (frequency)	Mass, damping and stiffness
Kostrzewsky et al. (1994)	HDJ	Bi-directional sine	Displ. (frequency)	Mass, damping and stiffness

References	Bearing type*	Type of excitation	Vibration response measured	Identified dynamic parameters
Ku (1994)	FTB	Sinusoidal	Displ. (frequency)	Damping and stiffness
Ku and Heshmat (1994)	Foil HDJ	Bi-directional sine	Displ., acc. (frequency)	Damping, stiffness and uncertainty
Tieu and Qiu (1994)	HDJ	Unbalance	Displ. (frequency)	Damping and stiffness
Xu (1994)	HYJ	Sinusoidal	Displ. (frequency)	Damping and stiffness
Zhang and Roberts (1994)	SQF	Sinusoidal	Displ. (frequency)	Non-linear force coefficients
Zhang et al. (1994)	SQF	Sinusoidal	Displacement (time)	Mass, damping and stiffness
Alexander et al. (1995)	AGS	PRBS	Displ., acc. (frequency)	Damping and stiffness
Arumugam et al. (1995)	HDJ	Uni-directional sine	Displ. (frequency)	Damping and stiffness
Chen and Lee (1995)	Ball	Unbalance	Displ. (frequency)	Damping and stiffness
Dmochowski and Brockwell (1995)	HDJ	Bi-directional sine	Displ., acc. (frequency)	Damping, stiffness and uncertainty
Franchek et al. (1995)	HYJ	PRBS	Displ., acc. (frequency)	Mass, damping and stiffness
Parkins (1995)	HDJ	Bi-directional sine	Velocity (time)	Damping and uncertainty
San Andrés et al. (1995)	HSJ	PRBS	Displ., acc. (frequency)	Mass, damping and stiffness
Santos (1995)	HDJ	Sinusoidal	Displ. (frequency)	Damping and stiffness
Taylor et al. (1995)	HDJ	Sinusoidal	Displ. (frequency)	Damping, stiffness and uncertainty
Tiwari and Vyas (1995, 1997a, 1998)	Ball	Random	Displ., vel. (time)	Non-linear stiffness
Childs and Gansle (1996)	AGS	Uni-directional sine	Displ., acc. (frequency)	Damping, stiffness and uncertainty
Ismail and Brown (1996)	ANS	Multi-frequency	Displ., vel., acc. (time)	Damping and stiffness
Kostrzewsky et al. (1996)	HDJ	Bi-directional sine	Displ. (frequency)	Damping, stiffness and uncertainty
Lee et al. (1996)	MB	Random	Current, volts, displ. (frequency)	Damping and stiffness Current stiffness
Qiu and Tieu (1996)	HDJ	Comp. sine	Displ. (frequency)	Damping, stiffness and uncertainty
Santos (1996)	HDJ	Sine sweep	Displ. (frequency)	Damping and stiffness
Vance and Li (1996)	DS	Impact	Displ. (time)	Damping
Zhang and Roberts (1996)	SQF	Sinusoidal	Displ. (frequency)	Mass and damping
Arumugam et al. (1997a, 1997b)	HDJ	Uni-directional sine	Displ. (frequency)	Damping, stiffness and uncertainty
Chen and Lee (1997)	Ball	Unbalance	Displ., vel. (time)	Damping and stiffness
Goodwin et al. (1997)	HDJ	PRBS	Displ. (frequency)	Damping and stiffness
Jiang et al. (1997)	HDJ	Impulse	Displ. (frequency)	Damping and stiffness
Marquette et al. (1997)	PLS	PRBS	Displ., acc. (frequency)	Mass, damping, stiffness and uncertainty
Marsh and Yantek (1997)	RB	Impact	Acc. (frequency)	Direct stiffness
Müller-Karger et al. (1997)	HDJ	Sinusoidal	Displ. (frequency)	Damping, stiffness and uncertainty
Prabhu (1997)	HDJ	Sinusoidal	Displ. (frequency)	Damping
Qiu and Tieu (1997)	HDJ	Impulse	Displ. (frequency)	Damping and stiffness
Reddy et al. (1997)	HDJ	Sinusoidal	Displ. (frequency)	Damping and stiffness
San Andrés and Childs (1997)	HSJ	PRBS	Displ., acc. (frequency)	Mass, damping, stiffness and uncertainty
Sawicki et al. (1997)	HYJ	Unbalance	Displ. (frequency)	Mass, damping, stiffness and uncertainty
Tiwari and Vyas (1997b)	Ball	Ran/unbalance	Displ., vel. (time)	Non-linear stiffness
Ismail and Brown (1998)	PLS	SPHS	Displ., acc. (time)	Mass, damping, stiffness and uncertainty
Kaneko et al. (1998)	ANS	Eccentric sleeves	Displ. (frequency)	Mass, damping, stiffness and uncertainty
Kostrzewsky et al. (1998)	HDJ	Bi-directional sine	Displ. (frequency)	Damping, stiffness and uncertainty
Mitsuya et al. (1998)	Ball	Impact	Displ. (frequency)	Damping and stiffness
Mosher and Childs (1998)	HYJ	PRBS	Displ., acc. (frequency)	Mass, damping, stiffness and uncertainty
Nikolakopoulos and Papadopoulos (1998)	HDJ (ER)	Incremental static load	Displacement	Stiffness
Royston and Basdogan (1998)	Ball	Random	Displ. (frequency)	Axial and radial stiffness
Yu and Childs (1998)	GS HCS	Uni-directional sine	Displ., acc. (frequency)	Damping, stiffness and uncertainty

References	Bearing type*	Type of excitation	Vibration response measured	Identified dynamic parameters
Childs and Fayolle (1999)	PLS	PRBS	Displ., acc. (frequency)	Mass, damping, stiffness and uncertainty
Fayolle and Childs (1999)	HYJ	PRBS	Displ., acc. (frequency)	Mass, damping, stiffness and uncertainty
Ha and Yang (1999)	HDJ	Bi-directional sine	Displ., acc. (frequency)	Damping and stiffness
Howard (1999)	FAB	Incremental static load	Displacement	Damping and stiffness
Kim and Lee (1999)	MB	Magnetic	Control current, displ.	Current and position stiffness
Laurant and Childs (1999)	HYJ	PRBS	Displ., acc. (frequency)	Mass, damping, stiffness and uncertainty
Li et al. (1999)	GDS	Impact	Displ. (frequency)	Damping and stiffness
Pettinato and Choudhury (1999)	HDJ	Incremental static load/unbalance	Displ. (frequency)	Damping, stiffness and uncertainty
Ransom et al. (1999)	GDS	Impact	Displ. (frequency)	Damping, stiffness and uncertainty
Soto and Childs (1999)	HCS	Swept sine	Displ., acc. (frequency)	Damping, stiffness and uncertainty
Wygant et al. (1999)	HDJ	Bi-directional sine	Displ. (frequency)	Damping, stiffness and uncertainty
Laos et al. (2000)	GDS	Periodic chirp	Displ., acc. (frequency)	Damping and uncertainty
Li et al. (2000)	GDS	Impact	Displ., acc. (frequency)	Damping and stiffness
Lindsey and Childs (2000)	PLS	PRBS	Displ., acc. (frequency)	Mass, damping, stiffness and uncertainty
Shamine et al. (2000)	RE	Impact	Acc. (frequency)	Stiffness and damping (tilt)
Tiwari (2000)	Ball	Random	Displ., vel. (time)	Non-linear stiffness
Vance and Ying (2000)	ER	Impact	Displacement (time)	Damping (0/2/0)
Zarzour and Vance (2000)	MD	Impact	Acc. (time)	Damping and stiffness
Howard et al. (2001)	FAB	Impact	Displacement (time)	Damping and stiffness (0/1/1)
Nielsen et al. (2001)	AGS	Swept-sine	Displ., acc. (frequency)	Damping, stiffness and uncertainty
Pettinato and Flack (2001)	HDJ	Bi-directional sine	Displ. (frequency)	Damping, stiffness and uncertainty
Pettinato et al. (2001)	HDJ	Bi-directional sine	Displ. (frequency)	Damping, stiffness and uncertainty
San Andrés et al. (2001)	SQF	Impact and sine	Displ., acc. (frequency)	Damping, stiffness and uncertainty
Tiwari et al. (2002)	SPR	Unbalance	Displ. (frequency)	Damping and stiffness
Dawson et al. (2002a, 2002b)	AGS	PRBS	Displ., acc. (frequency)	Damping, stiffness and uncertainty
Holt and Childs (2002)	AGS	PRBS	Displ., acc. (frequency)	Damping, stiffness and uncertainty
Laurant and Childs (2002)	HYJ	PRBS	Displ., acc. (frequency)	Mass, damping, stiffness and uncertainty
Vazquez et al. (2002)	SPR	Swept-sine	Acc. (frequency)	Damping and stiffness
Chatterjee and Vyas (2003)	Ball	Sinusoidal	Displ. (frequency)	Damping and non-linear stiffness
Kaneko et al. (2003)	ALS	Eccentric sleeves	Displ. (frequency)	Mass, damping, stiffness and uncertainty
Weatherwax and Childs (2003)	AGS	Eccentric sleeves	Displ., acc. (frequency)	Damping, stiffness and uncertainty

* The following abbreviations are used in the table: AGS, annular gas seal; ANS, annular seal; ALS, annular liquid seal; BS, brush seals; DS, damper seals; ER, electrorheological fluid; FAB, foil air; FTB, foil thrust; GDS, gas damper seal; GJ, gas journal; GS, gas seal; HCS, honeycombed seal; HDJ, hydrodynamic journal; HSJ, hydrostatic journal; HYJ, hybrid journal; LGS, long gas seal; LS, long seal; MB, magnetic; MD, metal mess bearing damper; PLS, plain liquid seal; RB, recirculating ball; RE, rolling element; SPR, springs; SQF, squeeze film; TPJ, tilting pad journal; TR, tapered roller.

APPENDIX B
GENERAL RIGID ROTOR SOLUTION 1

Input Rigid Rotor Parameters

$m := \frac{0.09748}{386}$ lbf-sec^2/in

$Ip := \frac{0.001616}{386}$ lbf-sec^2-in

$Id := \frac{1.889 \cdot 10^{-5}}{386}$ lbf-sec^2-in

$\Omega := 52359.9 \ \frac{rad}{sec}$

$a1 := 0.6$ inch

$a2 := -0.6$

$eu := 0.00000$ unbalance eccentricity, in

$eu\theta := \frac{\pi}{4}$

$\eta := eu \cdot \cos(eu\theta)$ $\zeta := eu \cdot \sin(eu\theta)$

$\eta = 1.41421 \times 10^{-6}$ $\zeta = 1.41421 \times 10^{-6}$

$Kyy1 := 2055.$	$Kyy2 := 2055.$	lbf/in	$Cyy1 := 0.01$	$Cyy2 := 0.01$	lbf-sec/in
$Kyz1 := 147.6$	$Kyz2 := 147.6$		$Cyz1 := -0.007$	$Cyz2 := -0.007$	
$Kzy1 := -91.36$	$Kzy2 := -91.36$		$Czy1 := 0.005$	$Czy2 := 0.005$	
$Kzz1 := 1713.1$	$Kzz2 := 1713.1$		$Czz1 := 0.035$	$Czz2 := 0.035$	

$$A := \begin{bmatrix} Kyy1 + Kyy2 - (\Omega)^2 \cdot m & Kyz1 + Kyz2 & a1 \cdot Kyz1 + a2 \cdot Kyz2 & -(a1 \cdot Kyy1 + a2 \cdot Kyy2) & \Omega \cdot (Cyy1 + Cyy2) & \Omega \cdot (Cyz1 + Cyz2) & \Omega \cdot (a1 \cdot Cyz1 + a2 \cdot Cyz2) & -\Omega \cdot (a1 \cdot Cyy1 + a2 \cdot Cyy2) \\ Kzy1 + Kzy2 & Kzz1 + Kzz2 - (\Omega)^2 \cdot m & a1 \cdot Kzz1 + a2 \cdot Kzz2 & -(a1 \cdot Kzy1 + a2 \cdot Kzy2) & \Omega \cdot (Czy1 + Czy2) & \Omega \cdot (Czz1 + Czz2) & \Omega \cdot (a1 \cdot Czz1 + a2 \cdot Czz2) & -\Omega \cdot (a1 \cdot Czy1 + a2 \cdot Czy2) \\ a1 \cdot Kzy1 + a2 \cdot Kzy2 & a1 \cdot Kzz1 + a2 \cdot Kzz2 & a1^2 \cdot Kyy1 + a2^2 \cdot Kzz2 - (\Omega)^2 \cdot Id & -\left(a1^2 \cdot Kzy1 + a2^2 \cdot Kzy2\right) & \Omega \cdot (a1 \cdot Czy1 + a2 \cdot Czy2) & \Omega \cdot (a1 \cdot Czz1 + a2 \cdot Czz2) & \Omega \cdot \left(a1^2 \cdot Cyy1 + a2^2 \cdot Czz2\right) & -\Omega \cdot \left(a1^2 \cdot Czy1 + a2^2 \cdot Czy2\right) + (\Omega)^2 \cdot Ip \\ -(a1 \cdot Kyy1 + a2 \cdot Kyy2) & -(a1 \cdot Kyz1 + a2 \cdot Kyz2) & -\left(a1^2 \cdot Kyz1 + a2^2 \cdot Kyz2\right) & a1^2 \cdot Kzz1 + a2^2 \cdot Kzz2 - (\Omega)^2 \cdot Id & -\Omega \cdot (a1 \cdot Cyy1 + a2 \cdot Cyy2) & -\Omega \cdot (a1 \cdot Cyz1 + a2 \cdot Cyz2) & -\Omega \cdot \left(a1^2 \cdot Cyz1 + a2^2 \cdot Cyz2\right) - (\Omega)^2 \cdot Ip & \Omega \cdot \left(a1^2 \cdot Czz1 + a2^2 \cdot Czz2\right) \\ -\Omega \cdot (Cyy1 + Cyy2) & -\Omega \cdot (Cyz1 + Cyz2) & -\Omega \cdot (a1 \cdot Cyz1 + a2 \cdot Cyz2) & \Omega \cdot (a1 \cdot Cyy1 + a2 \cdot Cyy2) & Kyy1 + Kyy2 - (\Omega)^2 \cdot m & Kyz1 + Kyz2 & a1 \cdot Kyz1 + a2 \cdot Kyz2 & -(a1 \cdot Kyy1 + a2 \cdot Kyy2) \\ -\Omega \cdot (Czy1 + Czy2) & -\Omega \cdot (Czz1 + Czz2) & -\Omega \cdot (a1 \cdot Czz1 + a2 \cdot Czz2) & \Omega \cdot (a1 \cdot Czy1 + a2 \cdot Czy2) & Kzy1 + Kzy2 & Kzz1 + Kzz2 - (\Omega)^2 \cdot m & a1 \cdot Kzz1 + a2 \cdot Kzz2 & -(a1 \cdot Kzy1 + a2 \cdot Kzy2) \\ -\Omega \cdot (a1 \cdot Czy1 + a2 \cdot Czy2) & -\Omega \cdot (a1 \cdot Czz1 + a2 \cdot Czz2) & -\Omega \cdot \left(a1^2 \cdot Cyy1 + a2^2 \cdot Czz2\right) & \Omega \cdot \left(a1^2 \cdot Czy1 + a2^2 \cdot Czy2\right) - (\Omega)^2 \cdot Ip & a1 \cdot Kzy1 + a2 \cdot Kzy2 & a1 \cdot Kzz1 + a2 \cdot Kzz2 & a1^2 \cdot Kzz1 + a2^2 \cdot Kzz2 - (\Omega)^2 \cdot Id & -\left(a1^2 \cdot Kzy1 + a2^2 \cdot Kzy2\right) \\ \Omega \cdot (a1 \cdot Cyy1 + a2 \cdot Cyy2) & \Omega \cdot (a1 \cdot Cyz1 + a2 \cdot Cyz2) & \Omega \cdot \left(a1^2 \cdot Cyz1 + a2^2 \cdot Cyz2\right) + (\Omega)^2 \cdot Ip & -\Omega \cdot \left(a1^2 \cdot Czz1 + a2^2 \cdot Czz2\right) & -(a1 \cdot Kyy1 + a2 \cdot Kyy2) & -(a1 \cdot Kyz1 + a2 \cdot Kyz2) & -\left(a1^2 \cdot Kyz1 + a2^2 \cdot Kyz2\right) & a1^2 \cdot Kyy1 + a2^2 \cdot Kyy2 - (\Omega)^2 \cdot Id \end{bmatrix}$$

$$RHS := m \cdot (\Omega)^2 \cdot \begin{pmatrix} \eta \\ \zeta \\ 0 \\ 0 \\ -\zeta \\ \eta \\ 0 \\ 0 \end{pmatrix}$$

(RHS unbalance forcing terms)

$$RHS = \begin{pmatrix} 0.09791 \\ 0.09791 \\ 0 \\ 0 \\ -0.09791 \\ 0.09791 \\ 0 \\ 0 \end{pmatrix}$$

$$A = \begin{pmatrix} -67306.42171 & 25.2 & 0 & 0 & 3141.594 & -429.35118 & 0 & 0 \\ 18.944 & -66987.02171 & 0 & 0 & 52.3599 & 3508.1133 & 0 & 0 \\ 0 & 0 & 617.62206 & -6.81984 & 0 & 0 & 1196.94731 & 11458.76585 \\ 0 & 0 & -9.072 & 675.11406 & 0 & 0 & -11323.04899 & 1262.92079 \\ -3141.594 & 429.35118 & 0 & 0 & -67306.42171 & 25.2 & 0 & 0 \\ -52.3599 & -3508.1133 & 0 & 0 & 18.944 & -66987.02171 & 0 & 0 \\ 0 & 0 & -1196.94731 & -11458.76585 & 0 & 0 & 675.11406 & -6.81984 \\ 0 & 0 & 11323.04899 & -1262.92079 & 0 & 0 & -9.072 & 560.13006 \end{pmatrix}$$

$q := A^{-1} \cdot RHS$

$$q = \begin{pmatrix} -1.37609 \times 10^{-6} \\ -1.53315 \times 10^{-6} \\ 0 \\ 0 \\ 1.50867 \times 10^{-6} \\ -1.37988 \times 10^{-6} \\ 0 \\ 0 \end{pmatrix}$$

Bearing Orbits

Bearing #1

$V1c := q_0 - a1 \cdot q_3$ $\qquad$ $W1c := q_1 + a1 \cdot q_2$

$V1s := q_4 - a1 \cdot q_7$ $\qquad$ $W1s := q_5 + a1 \cdot q_6$

Bearing #2

$V2c := q_0 - a2 \cdot q_3$ $\qquad$ $W2c := q_1 + a2 \cdot q_2$

$V2s := q_4 - a2 \cdot q_7$ $\qquad$ $W2s := q_5 + a2 \cdot q_6$

PLOT BEARING ORBITS

$T := \frac{2\cdot\pi}{\Omega}$ $\quad T = 0.00012$ $\quad t := 0, \frac{T}{200} .. T$

Bearing #1

$V1(t) := V1c\cdot\cos(\Omega\cdot t) + V1s\cdot\sin(\Omega\cdot t)$

$W1(t) := W1c\cdot\cos(\Omega\cdot t) + W1s\cdot\sin(\Omega\cdot t)$

Bearing #2

$V2(t) := V2c\cdot\cos(\Omega\cdot t) + V2s\cdot\sin(\Omega\cdot t)$

$W2(t) := W2c\cdot\cos(\Omega\cdot t) + W2s\cdot\sin(\Omega\cdot t)$

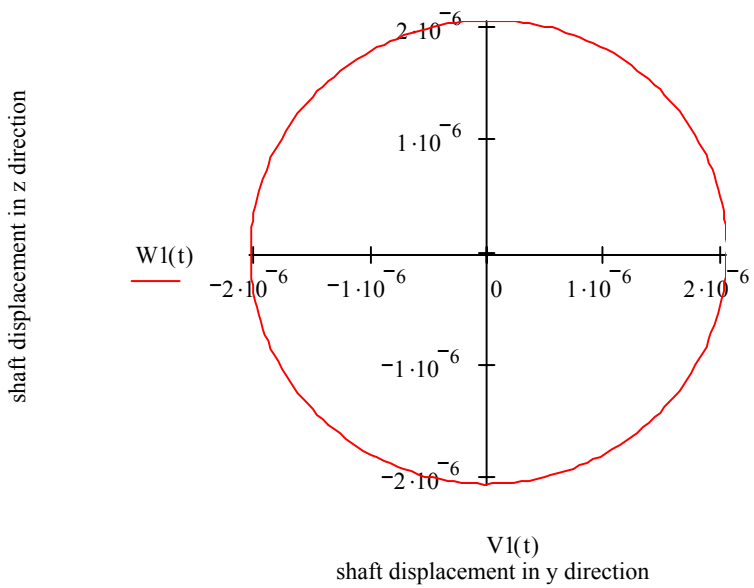

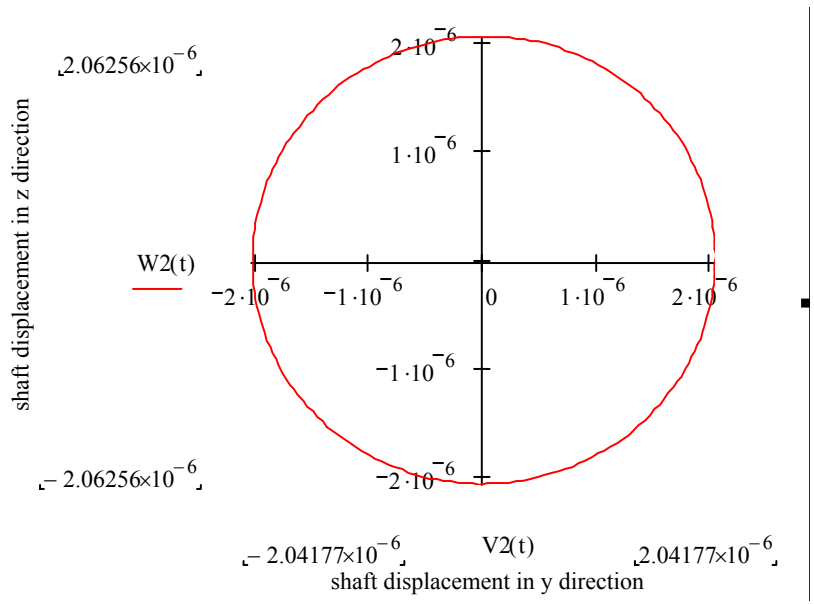

Work done per cycle at the bearings

Bearing #1

$$Kd1 := \frac{Kyz1 + Kzy1}{2} \qquad Cm1 := \frac{Cyy1 + Czz1}{2}$$

$$WK1Cir := 2 \cdot \pi \cdot Kd1 \cdot (V1c \cdot W1s - V1s \cdot W1c)$$

Work done by Circulation Force at Bearing #1

$$WK1Diss := -\pi \cdot \Omega \cdot \left[Cyy1 \cdot \left(V1c^2 + W1s^2 \right) + 2 \cdot Cm1 \cdot (V1c \cdot W1c + V1s \cdot W1s) + Czz1 \cdot \left(W1c^2 + W1s^2 \right) \right]$$

Work done by dissipation forces

$$WK1Total := WK1Cir + WK1Diss$$

Total work done at the bearing #1

Bearing #2

$$Kd2 := \frac{Kyz2 + Kzy2}{2} \qquad Cm2 := \frac{Cyy2 + Czz2}{2}$$

$$WK2Cir := 2 \cdot \pi \cdot Kd2 \cdot (V2c \cdot W2s - V2s \cdot W2c)$$

Work done by Circulation Force at Bearing #2

$$WK2Diss := -\pi \cdot \Omega \cdot \left[Cyy2 \cdot \left(V2c^2 + W2s^2 \right) + 2 \cdot Cm2 \cdot (V2c \cdot W2c + V2s \cdot W2s) + Czz2 \cdot \left(W2c^2 + W2s^2 \right) \right]$$

Work done by dissipation forces

$$WK2Total := WK2Cir + WK2Diss$$

Total work done at the bearing #2

Bearing #1

$WK1Cir = 4.13906 \times 10^{-11}$

$WK1Diss = -4.24666 \times 10^{-8}$

$WK1Total = -4.24253 \times 10^{-8}$

Bearing #2

$WK2Cir = 4.13906 \times 10^{-11}$

$WK2Diss = -4.24666 \times 10^{-8}$

$WK2Total = -4.24253 \times 10^{-8}$

NOTE: Total work done at each bearing/cycle must be negative(subtracting energy from rotor), for stable operation

APPENDIX C
GENERAL RIGID ROTOR SOLUTION 2

Input Rigid Rotor Parameters

$m := \frac{0.09748}{386}$ lbf-sec^2/in

$Ip := \frac{0.001616}{386}$ lbf-sec^2-in

$Id := \frac{1.889 \cdot 10^{-5}}{386}$ lbf-sec^2-in

$\Omega := 52359.9 \ \frac{rad}{sec}$

$a1 := 0.6$ inch

$a2 := -0.6$

$eu := 0.00000$ unbalance eccentricity, in

$eu\theta := \frac{\pi}{4}$

$\eta := eu \cdot \cos(eu\theta)$ $\zeta := eu \cdot \sin(eu\theta)$

$\eta = 1.41421 \times 10^{-6}$ $\zeta = 1.41421 \times 10^{-6}$

Bearing parameters found by using XLTiltPadHGB:

Kyy1 := 2055.3	Kyy2 := 2055.3	lbf/in	Cyy1 := 0.014	Cyy2 := 0.014	lbf-sec/in
Kyz1 := 147.6	Kyz2 := 147.6		Cyz1 := −0.0071	Cyz2 := −0.0071	
Kzy1 := −91.36	Kzy2 := −91.36		Czy1 := 0.005	Czy2 := 0.005	
Kzz1 := 1713.13	Kzz2 := 1713.13		Czz1 := 0.035	Czz2 := 0.035	

$$A := \begin{bmatrix} Kyy1 + Kyy2 - (\Omega)^2 \cdot m & Kyz1 + Kyz2 & a1 \cdot Kyz1 + a2 \cdot Kyz2 & -(a1 \cdot Kyy1 + a2 \cdot Kyy2) & \Omega \cdot (Cyy1 + Cyy2) & \Omega \cdot (Cyz1 + Cyz2) & \Omega \cdot (a1 \cdot Cyz1 + a2 \cdot Cyz2) & -\Omega \cdot (a1 \cdot Cyy1 + a2 \cdot Cyy2) \\ Kzy1 + Kzy2 & Kzz1 + Kzz2 - (\Omega)^2 \cdot m & a1 \cdot Kzz1 + a2 \cdot Kzz2 & -(a1 \cdot Kzy1 + a2 \cdot Kzy2) & \Omega \cdot (Czy1 + Czy2) & \Omega \cdot (Czz1 + Czz2) & \Omega \cdot (a1 \cdot Czz1 + a2 \cdot Czz2) & -\Omega \cdot (a1 \cdot Czy1 + a2 \cdot Czy2) \\ a1 \cdot Kzy1 + a2 \cdot Kzy2 & a1 \cdot Kzz1 + a2 \cdot Kzz2 & a1^2 \cdot Kyy1 + a2^2 \cdot Kzz2 - (\Omega)^2 \cdot Id & -(a1^2 \cdot Kzy1 + a2^2 \cdot Kzy2) & \Omega \cdot (a1 \cdot Czy1 + a2 \cdot Czy2) & \Omega \cdot (a1 \cdot Czz1 + a2 \cdot Czz2) & \Omega \cdot (a1^2 \cdot Cyy1 + a2^2 \cdot Czz2) & -\Omega \cdot (a1^2 \cdot Czy1 + a2^2 \cdot Czy2) + (\Omega)^2 \cdot Ip \\ -(a1 \cdot Kyy1 + a2 \cdot Kyy2) & -(a1 \cdot Kyz1 + a2 \cdot Kyz2) & -(a1^2 \cdot Kyz1 + a2^2 \cdot Kyz2) & a1^2 \cdot Kzz1 + a2^2 \cdot Kzz2 - (\Omega)^2 \cdot Id & -\Omega \cdot (a1 \cdot Cyy1 + a2 \cdot Cyy2) & -\Omega \cdot (a1 \cdot Cyz1 + a2 \cdot Cyz2) & -\Omega \cdot (a1^2 \cdot Cyz1 + a2^2 \cdot Cyz2) - (\Omega)^2 \cdot Ip & \Omega \cdot (a1^2 \cdot Czz1 + a2^2 \cdot Czz2) \\ -\Omega \cdot (Cyy1 + Cyy2) & -\Omega \cdot (Cyz1 + Cyz2) & -\Omega \cdot (a1 \cdot Cyz1 + a2 \cdot Cyz2) & \Omega \cdot (a1 \cdot Cyy1 + a2 \cdot Cyy2) & Kyy1 + Kyy2 - (\Omega)^2 \cdot m & Kyz1 + Kyz2 & a1 \cdot Kyz1 + a2 \cdot Kyz2 & -(a1 \cdot Kyy1 + a2 \cdot Kyy2) \\ -\Omega \cdot (Czy1 + Czy2) & -\Omega \cdot (Czz1 + Czz2) & -\Omega \cdot (a1 \cdot Czz1 + a2 \cdot Czz2) & \Omega \cdot (a1 \cdot Czy1 + a2 \cdot Czy2) & Kzy1 + Kzy2 & Kzz1 + Kzz2 - (\Omega)^2 \cdot m & a1 \cdot Kzz1 + a2 \cdot Kzz2 & -(a1 \cdot Kzy1 + a2 \cdot Kzy2) \\ -\Omega \cdot (a1 \cdot Czy1 + a2 \cdot Czy2) & -\Omega \cdot (a1 \cdot Czz1 + a2 \cdot Czz2) & -\Omega \cdot (a1^2 \cdot Cyy1 + a2^2 \cdot Czz2) & \Omega \cdot (a1^2 \cdot Czy1 + a2^2 \cdot Czy2) - (\Omega)^2 \cdot Ip & a1 \cdot Kzy1 + a2 \cdot Kzy2 & a1 \cdot Kzz1 + a2 \cdot Kzz2 & a1^2 \cdot Kzz1 + a2^2 \cdot Kzz2 - (\Omega)^2 \cdot Id & -(a1^2 \cdot Kzy1 + a2^2 \cdot Kzy2) \\ \Omega \cdot (a1 \cdot Cyy1 + a2 \cdot Cyy2) & \Omega \cdot (a1 \cdot Cyz1 + a2 \cdot Cyz2) & \Omega \cdot (a1^2 \cdot Cyz1 + a2^2 \cdot Cyz2) + (\Omega)^2 \cdot Ip & -\Omega \cdot (a1^2 \cdot Czz1 + a2^2 \cdot Czz2) & -(a1 \cdot Kyy1 + a2 \cdot Kyy2) & -(a1 \cdot Kyz1 + a2 \cdot Kyz2) & -(a1^2 \cdot Kyz1 + a2^2 \cdot Kyz2) & a1^2 \cdot Kyy1 + a2^2 \cdot Kyy2 - (\Omega)^2 \cdot Id \end{bmatrix}$$

$$RHS := m \cdot (\Omega)^2 \cdot \begin{pmatrix} \eta \\ \zeta \\ 0 \\ 0 \\ -\zeta \\ \eta \\ 0 \\ 0 \end{pmatrix}$$

(RHS unbalance forcing terms)

$$RHS = \begin{pmatrix} 0.09791 \\ 0.09791 \\ 0 \\ 0 \\ -0.09791 \\ 0.09791 \\ 0 \\ 0 \end{pmatrix}$$

$$A = \begin{pmatrix} -65124.42171 & 295.2 & 0 & 0 & 1466.0772 & -743.51058 & 0 & 0 \\ -182.72 & -65808.76171 & 0 & 0 & 523.599 & 3665.193 & 0 & 0 \\ 0 & 0 & 1222.46886 & 65.7792 & 0 & 0 & 923.62864 & 11289.11978 \\ 0 & 0 & -106.272 & 1099.28766 & 0 & 0 & -11209.95161 & 1319.46948 \\ -1466.0772 & 743.51058 & 0 & 0 & -65124.42171 & 295.2 & 0 & 0 \\ -523.599 & -3665.193 & 0 & 0 & -182.72 & -65808.76171 & 0 & 0 \\ 0 & 0 & -923.62864 & -11289.11978 & 0 & 0 & 1099.28766 & 65.7792 \\ 0 & 0 & 11209.95161 & -1319.46948 & 0 & 0 & -106.272 & 1345.65006 \end{pmatrix}$$

$$q := A^{-1} \cdot RHS$$

$$q = \begin{pmatrix} -1.46054 \times 10^{-6} \\ -1.5494 \times 10^{-6} \\ 0 \\ 0 \\ 1.51235 \times 10^{-6} \\ -1.39413 \times 10^{-6} \\ 0 \\ 0 \end{pmatrix}$$

Bearing Orbits

Bearing #1

$V1c := q_0 - a1 \cdot q_3$ $\quad$ $W1c := q_1 + a1 \cdot q_2$

$V1s := q_4 - a1 \cdot q_7$ $\quad$ $W1s := q_5 + a1 \cdot q_6$

Bearing #2

$V2c := q_0 - a2 \cdot q_3$ $\quad$ $W2c := q_1 + a2 \cdot q_2$

$V2s := q_4 - a2 \cdot q_7$ $\quad$ $W2s := q_5 + a2 \cdot q_6$

PLOT BEARING ORBITS

$T := \frac{2\cdot\pi}{\Omega}$ $\quad T = 0.00012$ $\quad t := 0, \frac{T}{200} .. T$

Bearing #1

$V1(t) := V1c\cdot\cos(\Omega\cdot t) + V1s\cdot\sin(\Omega\cdot t)$

$W1(t) := W1c\cdot\cos(\Omega\cdot t) + W1s\cdot\sin(\Omega\cdot t)$

Bearing #2

$V2(t) := V2c\cdot\cos(\Omega\cdot t) + V2s\cdot\sin(\Omega\cdot t)$

$W2(t) := W2c\cdot\cos(\Omega\cdot t) + W2s\cdot\sin(\Omega\cdot t)$

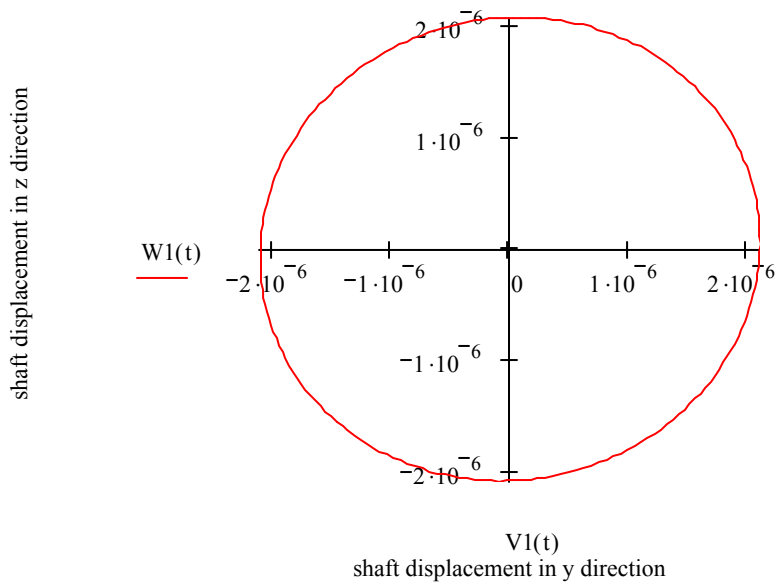

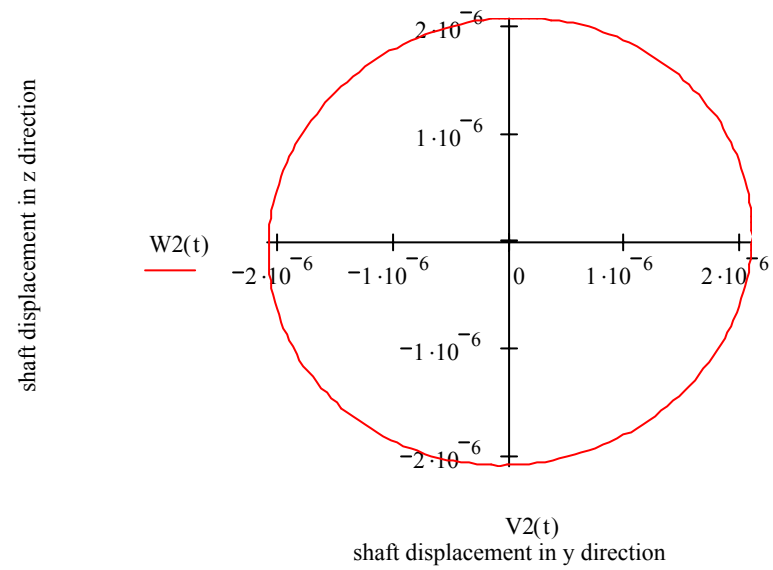

Work done per cycle at the bearings

Bearing #1

$$Kd1 := \frac{Kyz1 + Kzy1}{2} \qquad Cm1 := \frac{Cyy1 + Czz1}{2}$$

$$WK1Cir := 2 \cdot \pi \cdot Kd1 \cdot (V1c \cdot W1s - V1s \cdot W1c)$$

Work done by Circulation Force at Bearing #1

$$WK1Diss := -\pi \cdot \Omega \cdot \left[Cyy1 \cdot \left(V1c^2 + W1s^2 \right) + 2 \cdot Cm1 \cdot (V1c \cdot W1c + V1s \cdot W1s) + Czz1 \cdot \left(W1c^2 + W1s^2 \right) \right]$$

Work done by dissipation forces

$$WK1Total := WK1Cir + WK1Diss$$

Total work done at the bearing #1

Bearing #2

$$Kd2 := \frac{Kyz2 + Kzy2}{2} \qquad Cm2 := \frac{Cyy2 + Czz2}{2}$$

$$WK2Cir := 2 \cdot \pi \cdot Kd2 \cdot (V2c \cdot W2s - V2s \cdot W2c)$$

Work done by Circulation Force at Bearing #2

$$WK2Diss := -\pi \cdot \Omega \cdot \left[Cyy2 \cdot \left(V2c^2 + W2s^2 \right) + 2 \cdot Cm2 \cdot (V2c \cdot W2c + V2s \cdot W2s) + Czz2 \cdot \left(W2c^2 + W2s^2 \right) \right]$$

Work done by dissipation forces

$$WK2Total := WK2Cir + WK2Diss$$

Total work done at the bearing #2

Bearing #1

$WK1Cir = 7.73768 \times 10^{-10}$

$WK1Diss = -3.56451 \times 10^{-8}$

$WK1Total = -3.48713 \times 10^{-8}$

Bearing #2

$WK2Cir = 7.73768 \times 10^{-10}$

$WK2Diss = -3.56451 \times 10^{-8}$

$WK2Total = -3.48713 \times 10^{-8}$

NOTE: Total work done at each bearing/cycle must be negative (subtracting energy from rotor), for stable operation

APPENDIX D
EXAMPLE OF FINDING BEARING PARAMETERS

Let's choose two different speed, and different displacement components for each speed.

$\Omega := 2\cdot 10^4$ rad/sec

$a := 0.03$ $b := 0.01$ $g := 0.02$ $h := 0.03$

$\Omega 1 := 2.1\cdot 10^4$

$a1 := 0.036$ $b1 := 0.016$ $g1 := 0.026$ $h1 := 0.036$

$\theta := 0, 2\cdot\frac{\pi}{100} .. 2\cdot\pi$ where $\theta=\Omega t$

$y(\theta) := a\cdot\cos(\theta) + b\cdot\sin(\theta)$ $y1(\theta) := a1\cdot\cos(\theta) + b1\cdot\sin(\theta)$

$z(\theta) := g\cdot\cos(\theta) + h\cdot\sin(\theta)$ $z1(\theta) := g1\cdot\cos(\theta) + h1\cdot\sin(\theta)$

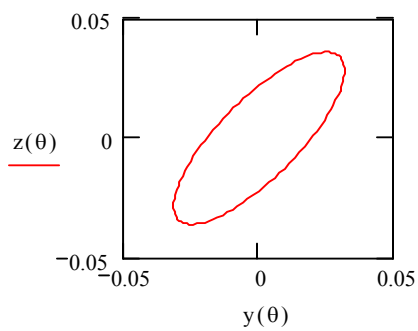

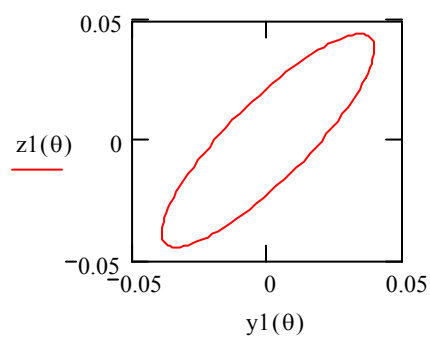

Let

$Kyy := 1000$ $Kzy := -500$ lbf/in $Cyy := 15$ $Czy := -4$ lbf-sec/in

$Kyz := 500$ $Kzz := 900$ $Cyz := 4$ $Czz := 15$

So by assuming all variables, forces can be find by using equation of motion (4-6), where

$Fy(\theta)=m*\cos(\theta)+n*\sin(\theta)$ and $Fz(\theta)=p*\cos(\theta)+q*\sin(\theta)$.

$$m := a\cdot Kyy + g\cdot Kyz + b\cdot\Omega\cdot Cyy + h\cdot\Omega\cdot Cyz \qquad m1 := a1\cdot Kyy + g1\cdot Kyz + b1\cdot\Omega1\cdot Cyy + h1\cdot\Omega1\cdot Cyz$$

$$n := b\cdot Kyy + h\cdot Kyz - a\cdot\Omega\cdot Cyy - g\cdot\Omega\cdot Cyz \qquad n1 := b1\cdot Kyy + h1\cdot Kyz - a1\cdot\Omega1\cdot Cyy - g1\cdot\Omega1\cdot Cyz$$

$$p := a\cdot Kzy + g\cdot Kzz + b\cdot\Omega\cdot Czy + h\cdot\Omega\cdot Czz \qquad p1 := a1\cdot Kzy + g1\cdot Kzz + b1\cdot\Omega1\cdot Czy + h1\cdot\Omega1\cdot Czz$$

$$q := b\cdot Kzy + h\cdot Kzz - a\cdot\Omega\cdot Czy - g\cdot\Omega\cdot Czz \qquad q1 := b1\cdot Kzy + h1\cdot Kzz - a1\cdot\Omega1\cdot Czy - g1\cdot\Omega1\cdot Czz$$

Now by using force and displacement components, lets find stiffness and damping coefficients.

$$P := \begin{pmatrix} b\cdot\Omega & h\cdot\Omega & a & g & 0 & 0 & 0 & 0 \\ -a\cdot\Omega & -g\cdot\Omega & b & h & 0 & 0 & 0 & 0 \\ 0 & 0 & 0 & 0 & b\cdot\Omega & h\cdot\Omega & a & g \\ 0 & 0 & 0 & 0 & -a\cdot\Omega & -g\cdot\Omega & b & h \end{pmatrix} \qquad T := \begin{pmatrix} m \\ n \\ p \\ q \end{pmatrix}$$

For each speed, there are set of four equations, expressed above. Thus for two different speeds, following expression is obtained:

$$P1 := \begin{pmatrix} b\cdot\Omega & h\cdot\Omega & a & g & 0 & 0 & 0 & 0 \\ -a\cdot\Omega & -g\cdot\Omega & b & h & 0 & 0 & 0 & 0 \\ 0 & 0 & 0 & 0 & b\cdot\Omega & h\cdot\Omega & a & g \\ 0 & 0 & 0 & 0 & -a\cdot\Omega & -g\cdot\Omega & b & h \\ b1\cdot\Omega1 & h1\cdot\Omega1 & a1 & g1 & 0 & 0 & 0 & 0 \\ -a1\cdot\Omega1 & -g1\cdot\Omega1 & b1 & h1 & 0 & 0 & 0 & 0 \\ 0 & 0 & 0 & 0 & b1\cdot\Omega1 & h1\cdot\Omega1 & a1 & g1 \\ 0 & 0 & 0 & 0 & -a1\cdot\Omega1 & -g1\cdot\Omega1 & b1 & h1 \end{pmatrix} \qquad T1 := \begin{pmatrix} m \\ n \\ p \\ q \\ m1 \\ n1 \\ p1 \\ q1 \end{pmatrix}$$

$$Ans := P1^{-1}\cdot T1 \qquad Ans = \begin{pmatrix} 15 \\ 4 \\ 1000 \\ 500 \\ -4 \\ 15 \\ -500 \\ 900 \end{pmatrix} \qquad \begin{pmatrix} Cyy \\ Cyz \\ Kyy \\ Kyz \\ Czy \\ Czz \\ Kzy \\ Kzz \end{pmatrix}$$

As it can be seen, stiffness and damping coefficients are the same values as assumed.

Let's assume force data were read in error, because of noise. Forces in y direction and forces in z direction are read in ten and four percent error, respectively.

$$m := m\cdot 1.1 \qquad n := n\cdot 1.1 \qquad p := p\cdot 1.04 \qquad q := q\cdot 1.04$$

$$m1 := m1\cdot 1.1 \qquad n1 := n1\cdot 1.1 \qquad p1 := p1\cdot 1.04 \qquad q1 := q1\cdot 1.04$$

$$P1 := \begin{pmatrix} b\cdot\Omega & h\cdot\Omega & a & g & 0 & 0 & 0 & 0 \\ -a\cdot\Omega & -g\cdot\Omega & b & h & 0 & 0 & 0 & 0 \\ 0 & 0 & 0 & 0 & b\cdot\Omega & h\cdot\Omega & a & g \\ 0 & 0 & 0 & 0 & -a\cdot\Omega & -g\cdot\Omega & b & h \\ b1\cdot\Omega 1 & h1\cdot\Omega 1 & a1 & g1 & 0 & 0 & 0 & 0 \\ -a1\cdot\Omega 1 & -g1\cdot\Omega 1 & b1 & h1 & 0 & 0 & 0 & 0 \\ 0 & 0 & 0 & 0 & b1\cdot\Omega 1 & h1\cdot\Omega 1 & a1 & g1 \\ 0 & 0 & 0 & 0 & -a1\cdot\Omega 1 & -g1\cdot\Omega 1 & b1 & h1 \end{pmatrix} \qquad T1 := \begin{pmatrix} m \\ n \\ p \\ q \\ m1 \\ n1 \\ p1 \\ q1 \end{pmatrix}$$

$$Ans := P1^{-1}\cdot T1 \qquad Ans = \begin{pmatrix} 16.5 \\ 4.4 \\ 1.1\times 10^{3} \\ 550 \\ -4.16 \\ 15.6 \\ -520 \\ 936 \end{pmatrix}$$

The result shows that the stiffness and damping coefficients are changed by the same percentage as forces. So it means noise in force affects bearing parameters at the same percentage as in force itself.

APPENDIX E
KISTLER DYNANOMETER

Force – FMD

KISTLER

P.
1 ... 4

3-Komponenten-Dynamometer F_x, F_y, F_z
Dynamomètre à 3 composantes F_x, F_y, F_z
3-Component Dynamometer F_x, F_y, F_z

Type

9257B, 9403

Quarzkristall-Dreikomponenten-Dynamometer zum Messen der drei orthogonalen Komponenten einer Kraft. Das Dynamometer besitzt eine grosse Steifheit und demzufolge eine hohe Eigenfrequenz. Das grosse Auflösungsvermögen ermöglicht das Messen von kleinsten dynamischen Änderungen grosser Kräfte.

Dynamomètre à cristal de quartz à trois composantes pour mesurer des trois composantes orthogonales d'une force. Le dynamomètre possède une grande rigidité et par conséquent une fréquence propre élevée. Sa très haute résolution permet de mesurer les moindres variations de larges forces.

Quartz three-component dynamometer for measuring the three orthogonal components of a force. The dynamometer has a great rigidity and consequently a high natural frequency. Its high resolution enables the smallest dynamic changes in large forces to be measured.

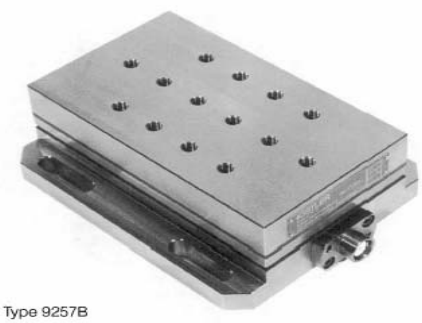

Type 9257B

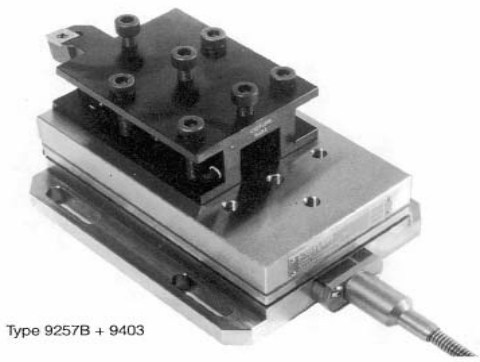

Type 9257B + 9403

Technische Daten	Données techniques	Technical Data			
Bereich F_z bei F_x und $F_y \leq 0{,}5\ F_z$	**Gamme** F_z pour F_x et $F_y \leq 0{,}5\ F_z$	**Range** F_z for F_x and $F_y \leq 0{,}5\ F_z$	F_x, F_y, F_z F_z	kN kN	–5 ... 5 *) –5 ... 10 **)
Kalibrierter Teilbereich 1	**Gamme partielle étalonnée 1**	**Calibrated partial range 1**	F_x, F_y F_z	N N	0 ... 500 0 ... 1000
Kalibrierter Teilbereich 2	**Gamme partielle étalonnée 2**	**Calibrated partial range 2**	F_x, F_y F_z	N N	0 ... 50 0 ... 100
Überlast F_z bei F_x und $F_y \leq 0{,}5\ F_z$	**Surcharge** F_z pour F_x et $F_y \leq 0{,}5\ F_z$	**Overload** F_z for F_x and $F_y \leq 0{,}5\ F_z$	F_x, F_y, F_z F_z	kN kN	–7,5/7,5 –7,5/15
Ansprechschwelle	**Seuil de réponse**	**Threshold**		N	<0,01
Empfindlichkeit	**Sensibilité**	**Sensitivity**	F_x, F_y F_z	pC/N pC/N	≈–7,5 ≈–3,7
Linearität, alle Bereiche **Hysterese,** alle Bereiche **Übersprechen**	**Linéarité,** toutes les gammes **Hystérésis,** toutes les gammes **Cross talk**	**Linearity,** all ranges **Hysteresis,** all ranges **Cross talk**		% FSO % FSO %	≤±1 ≤0,5 ≤±2
Steifheit	**Rigidité**	**Rigidity**	c_x, c_y c_z	kN/µm kN/µm	>1 >2
Eigenfrequenz **Eigenfrequenz** (montiert an Flanschen)	**Fréquence propre** **Fréquence propre** (installé sur brides)	**Natural frequency** **Natural frequency** (mounted on flanges)	f_o (x, y, z) f_o (x, y) f_o (z)	kHz kHz kHz	≈3,5 ≈2,3 ≈3,5
Betriebstemperaturbereich **Temperaturkoeffizient** der Empfindlichkeit	**Gamme de température d'utilisation** **Coefficient de température** de la sensibilité	**Operating temperature range** **Temperature coefficient** of sensitivity		°C %/°C	0 ... 70 –0,02
Kapazität (pro Kanal) **Isolationswiderstand** (20 °C) **Masseisolation**	**Capacité** (de canal) **Résistance d'isolement** (20 °C) **Isolé à la masse**	**Capacitance** (of channel) **Insulation resistance** (20 °C) **Ground insulation**		pF Ω Ω	≈220 $>10^{13}$ $>10^{8}$
Schutzart **Gewicht**	**Classe de protection** **Poids**	**Protection class** **Weight**		– kg	IP 67 ***) 7,3

*) Kraftangriff innerhalb und max. 25 mm oberhalb der Deckfläche.
**) Bereich beim Drehen, Kraftangriff bei Punkt A.
***) Mit Anschlusskabel Typen 1687B5, 1689B5

*) Point d'application de la force au-dedans et max. 25 mm au-dessus de la plaque supérieure.
**) Gamme lors du tournage, point d'application au point A.
***) Avec câble de connexion types 1687B5, 1689B5

*) Application of force inside and max. 25 mm above top plate area.
**) Range for turning, application of force at point A.
***) With connecting cable Types 1687B5, 1689B5

1 N (Newton) = 1 kg · m · s^{-2} = 0,1019... kp = 0,2248... lbf; 1 inch = 25,4 mm; 1 kg = 2,2046... lb; 1 Nm = 0,73756... lbft

Kistler Instrumente AG Winterthur, CH-8408 Winterthur, Switzerland, Tel. (052) 224 11 11 Kistler Instrument Corp., Amherst, NY 14228-2171, USA, Phone (716) 691-5100

Dynamometer Typ 9257B

Abmessungen

Dynamomètre type 9257B

Dimensions

Dynamometer Type 9257B

Dimensions

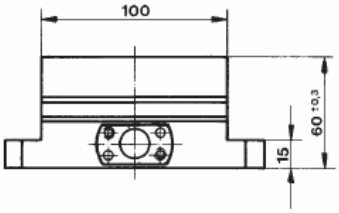

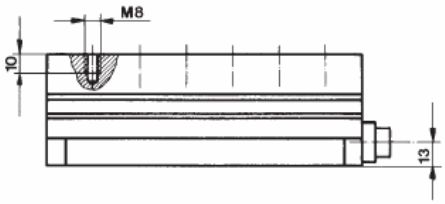

Fräsen, Schleifen
Fraisage, rectifiage
Milling, grinding

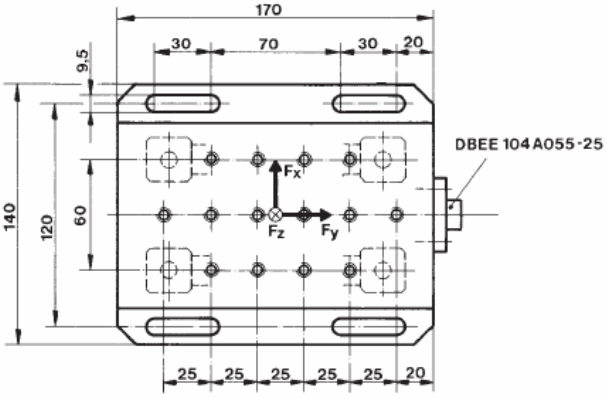

Dynamometer Typ 9257B

Abmessungen mit montiertem Stahlhalter

Stahlhalter	Typ 9403
Anschlusskabel	Typ 1687B5 / 1689B5

Dynamomètre type 9257B

Dimensions avec porte-outil monté

Porte-outil	type 9403
Câble de connexion	type 1687B5 / 1689B5

Dynamometer Type 9257B

Dimensions with mounted tool holder

Tool holder	Type 9403
Connecting cable	Type 1687B5 / 1689B5

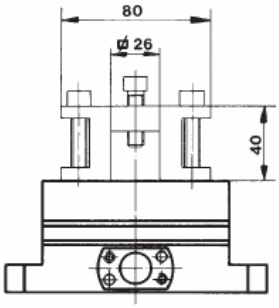

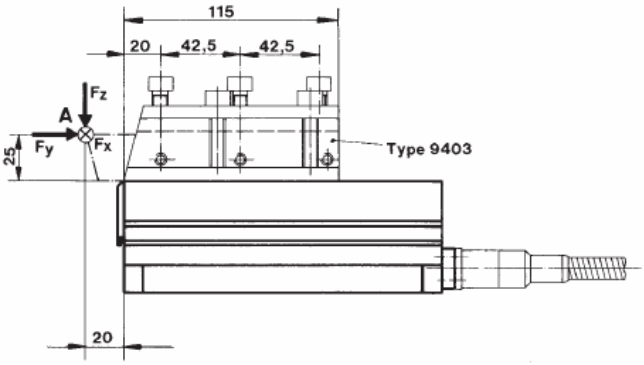

Drehen
Tournage
Turning

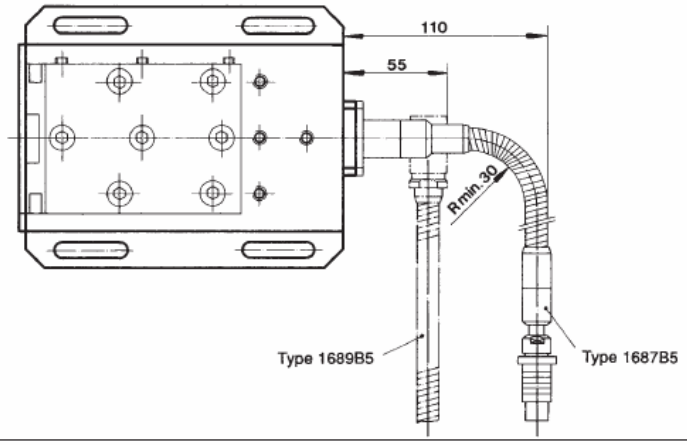

LIST OF REFERENCES

[1] Kussul, E. M., Rachkovskij, D. A., Baidyk, T. N., and Talayev, S. A., 1996, "Micromechanical engineering: A basis for the l0w-cost manufacturing for mechanical microdevices using microequipment," Journal of Micromechanical Microengineering, vol. 6, pp. 410–425.

[2] Masuzawa, T., and Tonshoff, H. K., 1997, "Three-dimensional micromachining by machine tools," Annals of the CIRP, vol. 46, pp. 621–628.

[3] Roy R. Craig, Jr., 1981, "Structural Dynamics," 1st edition, pp. 430-434.

[4] Tiwari, R., Lees, A. W., and Friswell, M. I., 2004, "Identification of Dynamic Bearing Parameters: A review," The Shock and Vibration Digest, vol. 36, pp. 99-124.

[5] Mitchell, J.R., Holmes, R., and Ballegooyen, H.V., 1965–66, "Experimental Determination of a Bearing Oil Film Stiffness," in Proceedings of the 4th Lubrication and Wear Convention, IMechE, Vol. 180, No. 3K, 90–96.

[6] Arumugam, P., Swarnamani, S., and Prabhu, B. S., 1995, "Experimental Identification of Linearized Oil Film Coefficients of Cylindrical and Tilting Pad Bearings," ASME Journal of Engineering for Gas Turbines and Power, Vol. 117, No. 3, 593–599.

[7] Glienicke, J., 1966–67, "Experimental Investigation of the Stiffness and Damping Coefficients of Turbine Bearings and Their Application to Instability Prediction," Proceedings of IMechE, Vol. 181, No. 3B, 116–129.

[8] Morton, P.G., 1971, "Measurement of the Dynamic Characteristics of Large Sleeve Bearing," ASME Journal of Lubrication Technology, Vol. 93, No.1, 143–150.

[9] Someya, T., 1976, "An Investigation into the Spring and Damping Coefficients of the Oil Film in Journal Bearing," Transactions of the Japan Society of Mechanical Engineers, Vol. 42, No. 360, 2599–2606.

[10] Hisa, S., Matsuura, T., and Someya, T., 1980, "Experiments on the Dynamic Characteristics of Large Scale Journal Bearings," in Proceedings of the 2nd International Conference on Vibration in Rotating Machinery, IMechE, Cambridge, UK, Paper C284, 223–230.

[11] Sakakida, H., Asatsu, S., and Tasaki, S., 1992, "The Static and Dynamic Characteristics of 23 Inch (584.2 mm) Diameter Journal Bearing," in Proceedings of the 5th International Conference on Vibration in Rotating Machinery, IMechE, Bath, UK, Paper C432/057, 351–358.

[12] Hagg, A.C., and Sankey, G.O., 1956, "Some Dynamic Properties of Oil-Film Journal Bearings with Reference to the Unbalance Vibration of Rotors," ASME Journal of Applied Mechanics, Vol. 78, No. 2, 302–305.

[13] Hagg, A.C., and Sankey, G.O., 1958, "Elastic and Damping Properties of Oil-Film Journal Bearings for Application to Unbalance Vibration Calculations," ASME Journal of Applied Mechanics, Vol. 80, No. 1, 141–143.

[14] Stone, J.M., and Underwood, A.F., 1947, "Load-Carrying Capacity of Journal Bearing," SAE Quarterly Transactions, Vol. 1, No. 1, 56–70.

[15] Duffin, S., and Johnson, B.T., 1966–67, "Some Experimental and Theoretical Studies of Journal Bearings for Large Turbine-Generator Sets," Proceedings of IMechE, Vol. 181, Part 3B, 89–97.

[16] Murphy, B.T., and Wagner, M.N., 1991, "Measurement of Rotordynamic Coefficients for a Hydrostatic Radial Bearing," ASME Journal of Tribology, Vol. 113, No. 3, 518–525.

[17] Adams, M.L., Sawicki, J.T., and Capaldi, R.J., 1992, "Experimental Determination of Hydrostatic Journal Bearing Rotordynamic Coefficients," in Proceedings of the 5th International Conference on Vibration in Rotating Machinery, IMechE, Bath, UK, Paper C432/145, 365–374.

[18] Sawicki, J.T., Capaldi, R.J., and Adams M.L., 1997, "Experimental and Theoretical Rotordynamic Characteristics of a Hybrid Journal Bearing," ASME Journal of Tribology, Vol. 119, No. 1, 132–142.

[19] Downham, E., and Woods, R., 1971, "The Rationale of Monitoring Vibration on Rotating Machinery in Continuously Operating Process Plant," in ASME Vibration Conference, Paper No. 71-Vibr-96.

[20] Nordmann, R., 1975, "Identification of Stiffness and Damping Coefficients of Journal Bearings by Means of the Impact Method," in Dynamics of Rotors: Stability and System Identification, O. Mahrenholtz, ed., Springer-Verlag, New York, 395–409.

[21] Nordmann, R., and Schöllhorn, K., 1980, "Identification of Stiffness and Damping Coefficients of Journal Bearings by Means of the Impact Method," in Proceedings of the 2nd International Conference on Vibration in Rotating Machinery, IMechE, Cambridge, UK, Paper C285, 231–238.

[22] Zhang, Y.Y., Xie, Y.B., and Qiu, D.M., 1992a, "Identification of Linearized Oil-Film Coefficients in a Flexible Rotor-Bearing System, Part I: Model and Simulation," Journal of Sound and Vibration, Vol. 152, No. 3, 531–547.

[23] Adams, M.L., and Rashidi, M, 1985, "On the Use of Rotor-Bearing Instability Thresholds to Accurately Measure Bearing Rotordynamic Properties," ASME Journal of Vibration, Acoustics, Stress, and Reliability in Design, Vol. 107, No. 4, 404–409.

[24] Lee, A.C., and Shih, Y.P., 1996, "Identification of the Unbalance Distribution and Dynamic Characteristics of Bearings in Flexible Rotors," Proceedings of IMechE, Part C: Journal of Mechanical Engineering Science, Vol. 210, No. 5, 409–432.

[25] Lund, J.W., Cheng, H.L., and Pan, H.T., 1965, "Rotor-Bearing Dynamic Design Technology, Part 3," Mechanical Technology.

BIOGRAPHICAL SKETCH

The author of the thesis was born on July 2, 1981, in Azerbaijan. He grew up in Azerbaijan. In 1998 he moved to Turkey to attend Middle east Technical University, where he received his Bachelor of Science in Mechanical Engineering. In 2004 he traveled to United States of America for the pursuit of a master's degree in mechanical engineering at University of Florida. He is planning to complete the degree of Master of Science in Mechanical Engineering in August 2006.